SEMI-ANNUAL STATUS REPORT

May 1987 - October 1987

for

NASA Grant NSG 1419

THE STRUCTURE OF SEPARATED FLOW REGIONS OCCURRING NEAR THE LEADING EDGE OF AIRFOILS INCLUDING TRANSITION

Thomas J. Mueller
Principal Investigator

Department of Aerospace and Mechanical Engineering
University of Notre Dame
Notre Dame, Indiana 46556

October 1987

SEMI-ANNUAL STATUS REPORT

May 1987 - October 1987

for

NASA GRANT NSG 1419*

All the time and effort during this report period was directed toward acquiring, reducing, and analyzing more hot-wire anemometer data. Some static pressure distribution data were also acquired to support the analysis of the velocity profile data. Laser Doppler Velocimetry data was not acquired due to equipment problems. The study included seven combinations of chord Reynolds number, angle of attack, and acoustic forcing using the NACA 66_3-018 airfoil.

This research has as its objective the detailed documentation of the structure and behavior of the transitional separation bubble and the redeveloping boundary layer after reattachment over an airfoil at low Reynolds numbers. The intent of this work is to further the understanding of the complex flow phenomena so that analytic methods for predicting their formulation and development can be improved. These analytic techniques have applications in the design and performance prediction of airfoils operating in the low Reynolds number flight regime.

---

*NASA Technical Monitor for this Grant is

Mr. Dan M. Somers, NASA Langley Research Center

Hampton, Virginia 23665.

REPEATABILITY OF PREVIOUS DATA

In order to test new equipment and software and gain confidence in the experimental techniques, hot-wire anemometer measurements were repeated for three cases previously studied by O'Meara [reference 1], namely α=12°, 0 flow restrictors, at R_C=140,000, 160,000, and 200,000. The results for the R_C=140,000 case are plotted with the corresponding O'Meara data in Figure 1. Since more points were measured within the separation bubble and the shear layer than in O'Meara's experiments, the magnitude and apparent shape of the recirculation zone are clear. The agreement between the two sets of U/U_{ext} data is good (within the 0.1 mm uncertainty of the height of the first point in the profile) except in the transition through reattachment profiles, x/c=7.0 to 10%.

These differences become clearer in the displacement thickness development for the three Reynolds numbers shown in Figures 2, 3, and 4. In all three cases, there is a sharp rise in the displacement thickness after separation. The displacement thickness reaches a local maximum at the chordwise position coincident with a sharp rise in momentum and energy thicknesses for the R_C=200,000 case and all the O'Meara cases. Brendel [reference 2] took this behavior to correspond to the transition point. After transition, δ_1 decreases until reattachment. Downstream of reattachment, δ_1 begins to grow again, continuing through the trailing edge of the airfoil. Although the Fitzgerald and O'Meara cases agree well for the R_C=200,000 case, (ie., within the uncertainty), for the R_C=140,000 and 160,000 cases, the δ_1's measured by Fitzgerald reach two local maximums, both aft of the local maximums in the corresponding O'Meara measurements. The second local maximum in both cases, however, may be due to uncertainty in the measurements. In any case, the Fitzgerald δ_1's decrease at a

slower rate than the corresponding O'Meara displacement thicknesses. This may be due to a poor seal in the floor of the test section through which the hot-wire probe was extended. Static pressure distributions measured for all three R_C cases for the unsealed and sealed slots are shown in Figures 5, 6, and 7. In all three cases, the effect of sealing the test section is to allow a faster pressure recovery after the bubble. As the R_C is increased from 140,000 to 200,000, the pressure recovery for both sealed and unsealed cases is faster as is suggested by the displacement thickness data. The difference in δ_1 can probably be attributed to the sealing problem.

The U/U_{ext} velocity profiles agree well with O'Meara's data. When the same data is plotted as U/U_{fs}, however, as shown in Figure 8 for the R_C=140,000, α=12°, 0 flow restrictors case, the velocity is seen to reach a different value at the edge of the boundary layer than the corresponding O'Meara case. In this and the R_C=200,000 cases, the velocity ratio is approximately 10% lower than the corresponding O'Meara cases while it is approximately 10% higher for the R_C=160,000 (α=12°, 0 flow restrictors) case. O'Meara observed this same type of discrepancy in his long-term repeatability tests [reference 1]. He suspected that probe calibration or orientation or changes in atmospheric conditions between tests may have caused this. Static pressure distribution measurements were taken to investigate this problem but have not shed any light on the cause of these discrepancies.

ACOUSTIC FORCING OF THE SEPARATION BUBBLE

Acoustic forcing of the separation bubble was conducted as a possible method of determining reverse flow regions when taking hot-wire measurements as well as to determine the effect of forcing on the separated shear layer and the development of the separation bubble. Hot-wire measurements were taken on an NACA 66_3-018 airfoil at R_c=140,000, α=10°, 0 flow restrictors for unforced and acoustically forced at 1623 Hz (fundamental), 770 Hz (subharmonic) and both 1541 and 770 Hz.

Acoustic forcing is an attempt to "lock" the early stages of transition into a repeatable, periodic, mode. When transition occurs naturally, the initial roll-up of the separated shear layer is modulated over a band of frequencies. Acoustic forcing at a dominant frequency within the flow focuses energy into a narrow band of frequencies. Thus, random motions may be "locked" into an easily recognizable frequency as shown by the hot-wire traces in figures 9 (unforced) and 10 (forced). When a hot-wire measures intermittent reverse flow, the signal is rectified. Thus, for a flow oscillating at a known frequency, the signal rectification inherent in hot-wire anemometry would return a signal that appears to be twice the known frequency. It was hypothesized that by acoustically forcing the bubble at a natural frequency, the reverse flow regions of the bubble could be determined by locating rectified portions of the hot-wire signal. The velocity data affected by rectification could then be corrected.

In order to determine a suitable forcing frequency, hot-wire data for an unforced case was taken along the upper surface of the airfoil. At each

point of each profile within the bubble, spectra were taken and integrated across the profile. This produced a series of spectra showing the spatial growth of dominant frequencies within the bubble. The most substantial peak occurred at x/c=7% as shown in Figure 11. The peak covered a band of frequencies centered around 1700 Hz. Thus, 1700 Hz was chosen as a first approximation to the fundamental frequency. With the hot-wire in the shear layer at x/c=7%, the bubble was acoustically forced and the forcing frequency "tuned" to 1666.67 Hz. This frequency was then designated the "fundamental" frequency since this was suspected to coincide with an initial shear layer roll up, if any [reference 3]. Similarly, one half the fundamental frequency, or 833 Hz was designated the "subharmonic" and twice the fundamental, or 3333 Hz was designated the "harmonic". Data taking was phase-locked with the forcing signal for all acoustic forcing cases. (The actual forcing frequencies used were 770 Hz instead of 833 Hz for the subharmonic and 1623 and 1541 Hz instead of 1666.67 Hz for the fundamental; the desired signals could not be produced by the phase-locking computer software.) The effect of the forcing is shown in the spectra given in Figures 11 and 12 for unforced and forced boundary layers, respectively, at x/c=7%. The forcing focuses the energy into the fundamental and first harmonic frequencies.

Hot-wire traces for the unforced and acoustically forced bubble are shown in Figures 9 and 10. Note that in the figures, the mean has been subtracted and that each trace is scaled on the largest signal within the profile. For both cases in the laminar portion of the bubble, the signal is dominated by low frequency oscillations probably due to spanwise velocity variations of the three-dimensional structure of the bubble. Superimposed on the low frequency

oscillations in both cases are higher frequency oscillations. These oscillations are more regular and have a higher amplitude for the acoustically forced case. With increasing x/c, the higher frequency oscillations dominate. For the unforced case, low frequency modulations occur in the traces which may again be due to spanwise velocity variations. The forced case is again much more regular and the effect of the forcing can be seen throughout the boundary layer. With increasing x/c, the oscillations become increasingly irregular until the flow is completely turbulent.

As a method of determining reverse flow regions, acoustic forcing has so far been unsuccessful. The fundamental frequency chosen in these cases is so high that rectifications have been hard to identify. Although higher frequencies dominate with increasing x/c, the low frequency modulations superposed on the fundamental and subharmonic are enough to hamper detection of rectified portions of the hot-wire signal. For the cases considered, the fundamental frequency was determined (tuned) at a point in the shear layer at an x/c of 7%. Since the dominant frequency changes with x/c and even within each profile, the velocity fluctuations are best "focused" near the center of the shear layer at x/c=7%; the influence of the forcing varies throughout the boundary layer. Finally, due to the proximity of the bubble to the airfoil's leading edge, the boundary layer is so small that measurements are difficult. Some of these problems may be overcome by using different techniques for analyzing this data.

Another difficulty with reverse flow determination by acoustic forcing technique is that the forcing may also affect the flowfield under consideration. Although changing the flowfield by acoustic forcing may prove beneficial to airfoil performance, reverse flow regions for the forced and unforced cases may

not coincide. A comparison of the hot-wire velocity profiles for the unforced and 1623 Hz forced cases is given in Figure 13. The differences between the two sets of profiles are well within the uncertainty from x/c=2 to 6%. For x/c > 7%, however, the velocity profiles are markedly different. The boundary layer transitions and reattaches roughly 2% x/c sooner when the bubble has been acoustically forced. By x/c=9% the forced shear layer has reattached while a significant bubble still exists for the unforced case.

The effect of 1623 Hz forcing on this bubble is also seen in the development of the displacement, momentum, and energy thicknesses as shown in Figure 14. The displacement thickness for the forced case follows the same trends as for the unforced case except that is appears to transition 0.5% x/c sooner and grows only slightly more than half the size of the unforced case. Thus, although δ_1 decreases at approximately the same rate for both cases, δ_1 for the forced case is only about 2/3 the thickness at x/c=13% for the unforced case.

The forcing helps channel the energy more efficiently than in the natural transition process. Transition is therefore accelerated, and reattachment occurs sooner. Acoustic forcing at a fundamental frequency of the shear layer also affects δ_2 and δ_3 growth. As shown in the figure, δ_2 and δ_3 for the forced and unforced cases agree well until x/c=6 or 7% when for the forced case δ_2 and δ_3 begin their growth corresponding to transition. The growth rate of δ_2 and δ_3 for the forced case, however, is significantly smaller than that for the unforced case, making determination of the beginning point of this growth difficult and resulting in thicknesses after reattachment for the forced cases only 75% as thick as the corresponding thicknesses of the unforced cases.

That acoustic forcing could affect the separation bubble is not surprising. In kerosene vapor flow visualization and titanium tetrachloride flow visualization experiments on the separation bubble, Schmidt observed the roll-up of the separated shear layer [reference 4]. It was hypothesized that the separated shear layer of the separation bubble might behave like a free shear layer or mixing layer. Because subharmonic and bimodal (both fundamental and subharmonic) frequency forcing has been shown to allow some control on shear layer roll-up and vortex pairing [reference 3], the bubble was also forced at the first subharmonic of the fundamental, 770 Hz, as well as bimodally at frequencies of 770 and 1541 Hz. The 770 Hz forcing had no noticeable effect on the boundary layer profiles or integrated thicknesses. Likewise, the bimodal forcing had nearly the same effect as forcing at 1623 Hz only; all these effects were therefore attributed to the 1541 Hz component of the forcing signal.

The change in modal energy with chordwise position was also explored for each frequency integrated over each profile. As expected from the e^n theories of Smith and Gramberoni and of van Ingen, [reference 5] the amplitude of each disturbance is seen to grow nearly linearly at least four orders of magnitude before saturating. As expected for vortex pairing, first the fundamental energy rises to saturation followed by the subharmonic and first harmonic [reference 6]. Unexpectedly, however, the harmonic and subharmonic both saturate below the saturation energy of the fundamental. The effect of the forcing may be to accelerate the most susceptable instabilities or roll-up frequencies. This would encourage the flow breakdown into turbulence and consequently shorten the bubble length and boundary layer thickness as noted above. Thus, acoustic forcing should also affect the lift and drag characteristics of the airfoil.

CONCLUSION

Although the U/U_{ext} profiles for the cases measured by O'Meara have been fairly repeatable, the source of discrepancies in U/U_{fs} profiles is still under investigation. The first attempts at determining reverse flow regions on the NACA 66_3-018 airfoil by acoustic forcing have not worked as well as initially hoped. Another researcher at Notre Dame has had more promising results, albeit on a different airfoil with a different separation bubble. In addition, the effect of acoustic forcing on the bubble at a fundamental frequency has been seen to shorten the bubble and make the boundary layer thinner. More research needs to be done then to better document the effects of acoustic forcing as well as continuing to study the unforced case. These will aid in the understanding of the transition process and the separation bubble flowfield in particular.

REFERENCES

1. O'Meara, M.M., "An Experimental Investigation of the Separation Bubble Flow Field Over an Airfoil at Low Reynolds Numbers", M.S. Thesis, University of Notre Dame, 1985.

2. Brendel, M., "Boundary Layer Measurements on an Airfoil at Low Reynolds Numbers," AIAA 87-0495, 1987. To be published in Journal of Aircraft.

3. Bradley, T.A., and Ng, T.T., "Phase-Locking in a Jet Forced with Two Frequencies," submitted to Experiments in Fluids.

4. Schmidt, G.S., "The Prediction of Transitional Separation Bubbles at Low Reynolds Numbers," Ph.D. Dissertation, University of Notre Dame, 1986.

5. White, F.M., Viscous Fluid Flow, McGraw-Hill, Inc., 1974.

6. Cain, A.B., and Thompson, M.W., "Linear and Weakly Nonlinear Aspects of Free Shear Layer Instability, Roll-up, Subharmonic Interaction and Wall Influence," AIAA 86-1047, 1986.

NOMENCLATURE

c	Airfoil Chord
Cp	Pressure coefficient, $Cp=(P_i-P_{fs})/Q_{fs}$
E(f)	Spectral energy at a given frequency f
FR	Flow Restrictor
I	Integrated spectral energy (in a profile), $I=\int_0^t E(f)dy$
R_c	Chord Reynolds number
U	Local velocity
U_{fs}	Freestream velocity
U_{ext}	External velocity
x/c	Nondimensional distance along chord
y	Height above airfoil surface, mm

Greek Symbols:

α	Angle of attack
δ	Boundary layer thickness
δ_1	Boundary layer displacement thickness
δ_3	Boundary layer energy thickness
δ_2	Boundary layer momentum thickness
ν	Kinematic viscosity

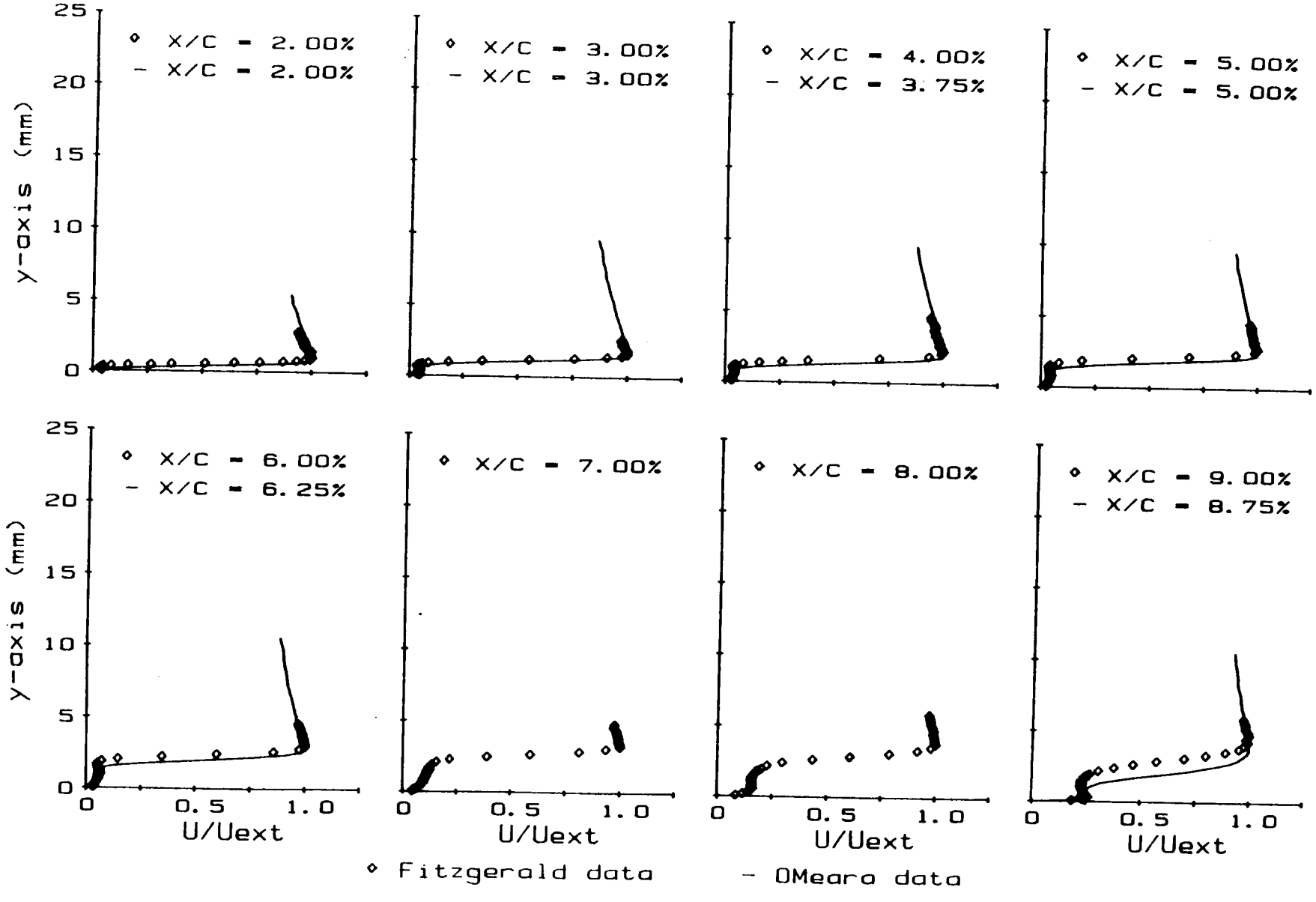

Figure 1a. Non-Dimensional Velocity Profiles (U/U_{ext}), x/c = 2.- 9.%, R_c = 140,000, α = 12°, 0 Flow Restrictors.

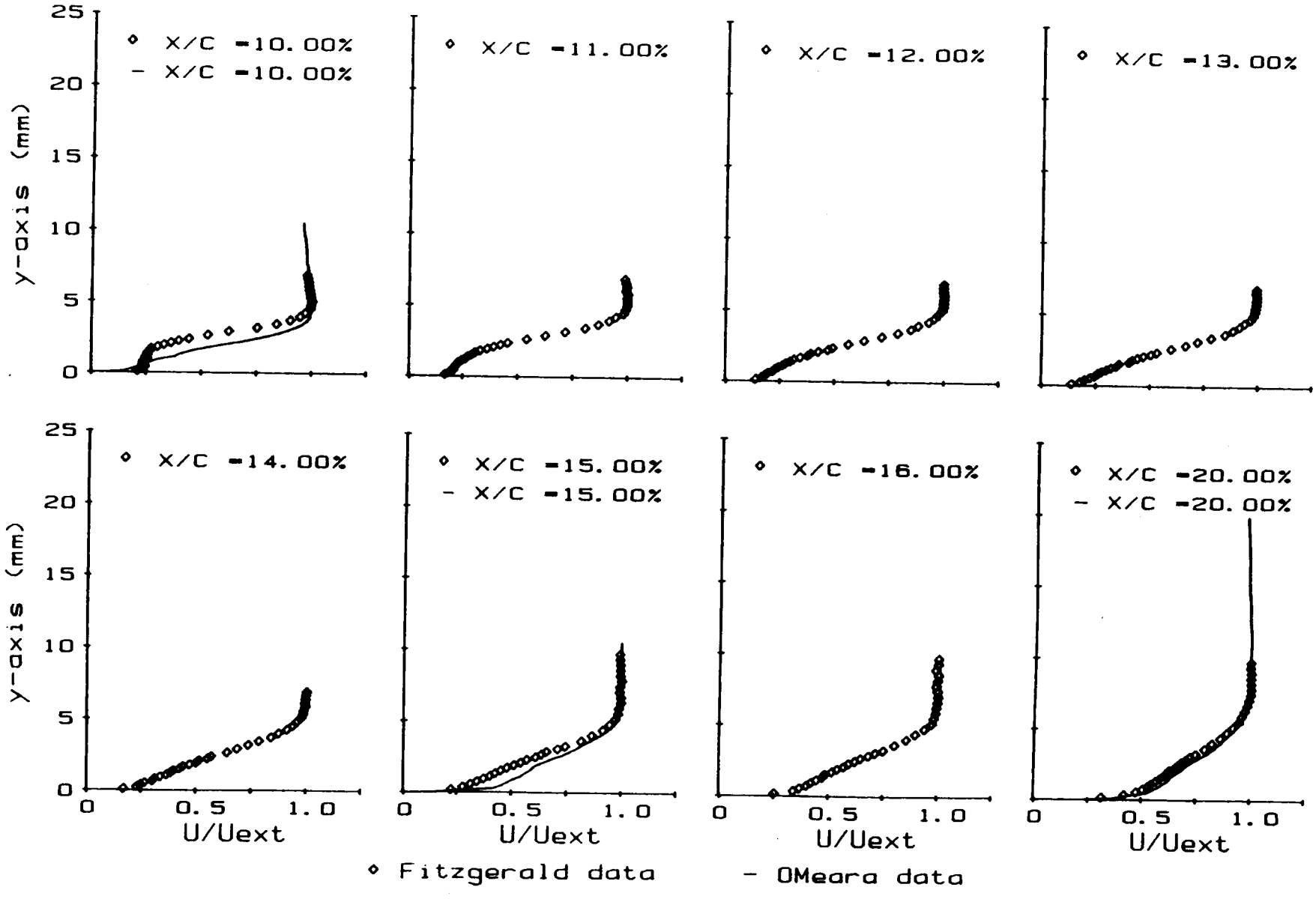

Figure 1b. Non-Dimensional Velocity Profiles (U/U_{ext}), x/c =10.- 20.%, R_c = 140,000, α = 12°, 0 Flow Restrictors.

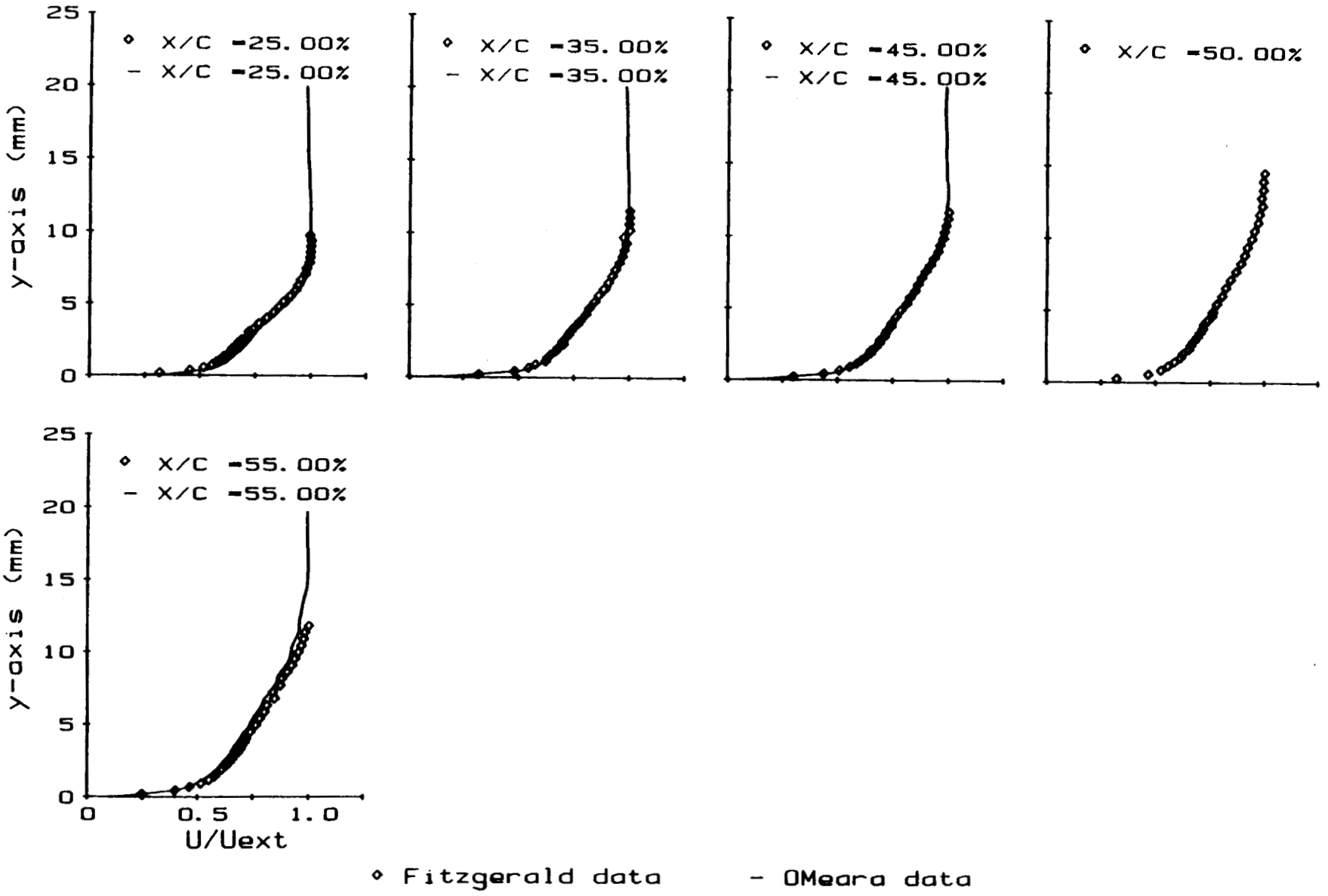

Figure 1c. Non-Dimensional Velocity Profiles (U/U_{ext}), x/c = 25.- 55.%, R_c = 140,000, α = 12°, 0 Flow Restrictors.

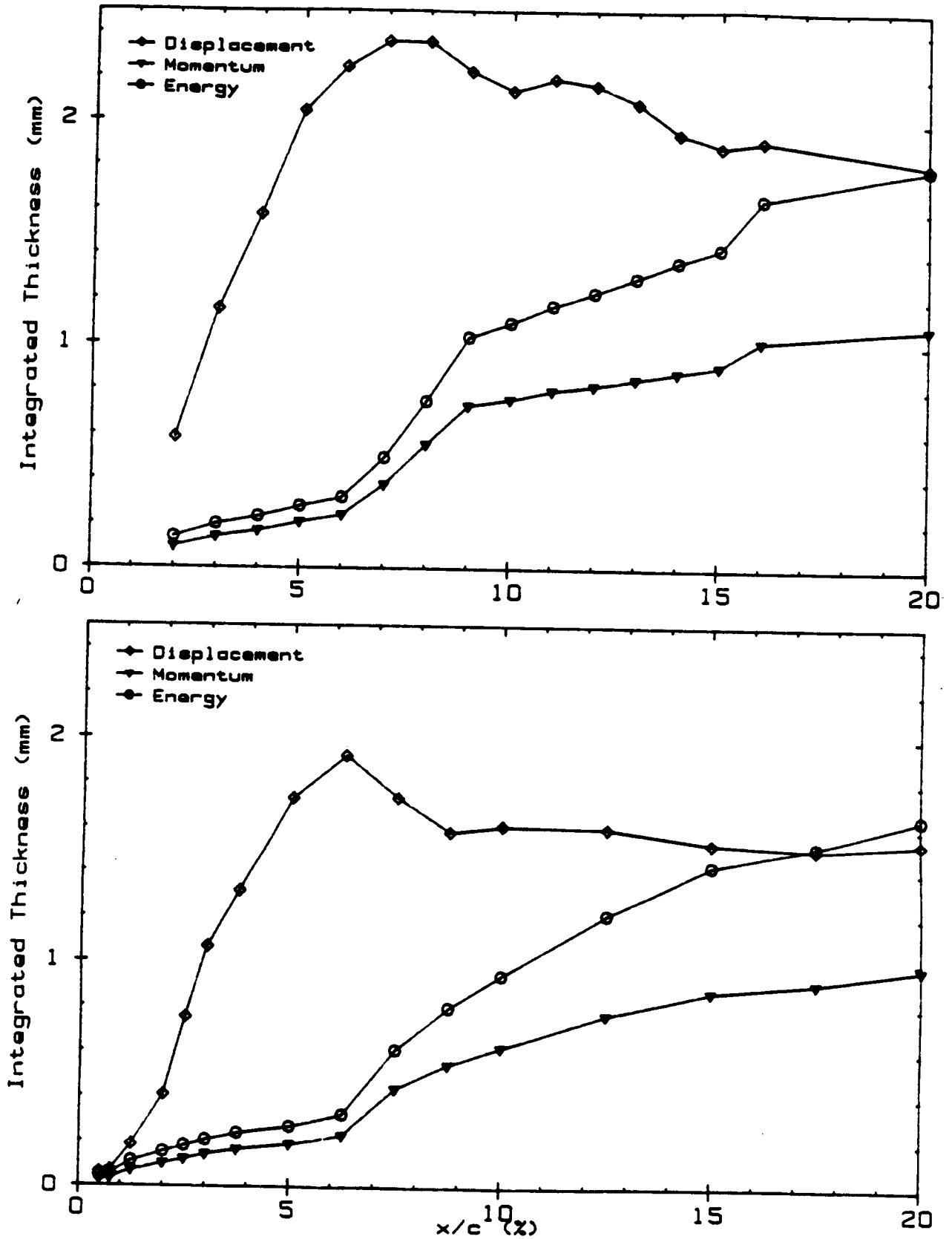

Figure 2. Integrated Boundary Layer Parameters on NACA 66_3-018 Airfoil, R_c= 140,000, α = 12°, 0 Flow Restrictors; Fitzgerald Data (top), O'Meara Data (bottom).

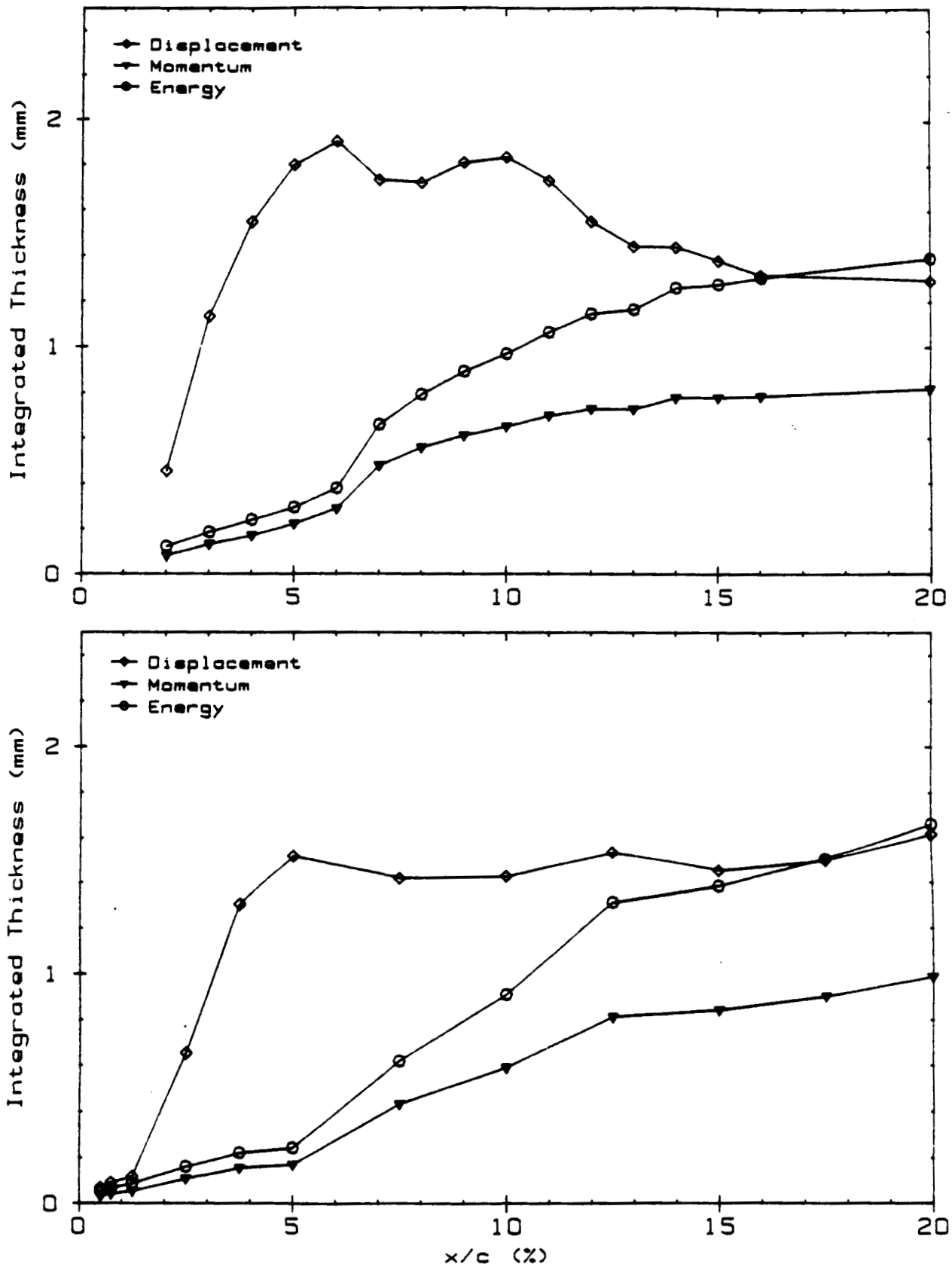

Figure 3. Integrated Boundary Layer Parameters on NACA 66_3-018 Airfoil, R_c= 160,000, α = 12°, 0 Flow Restrictors; Fitzgerald Data (top), O'Meara Data (bottom).

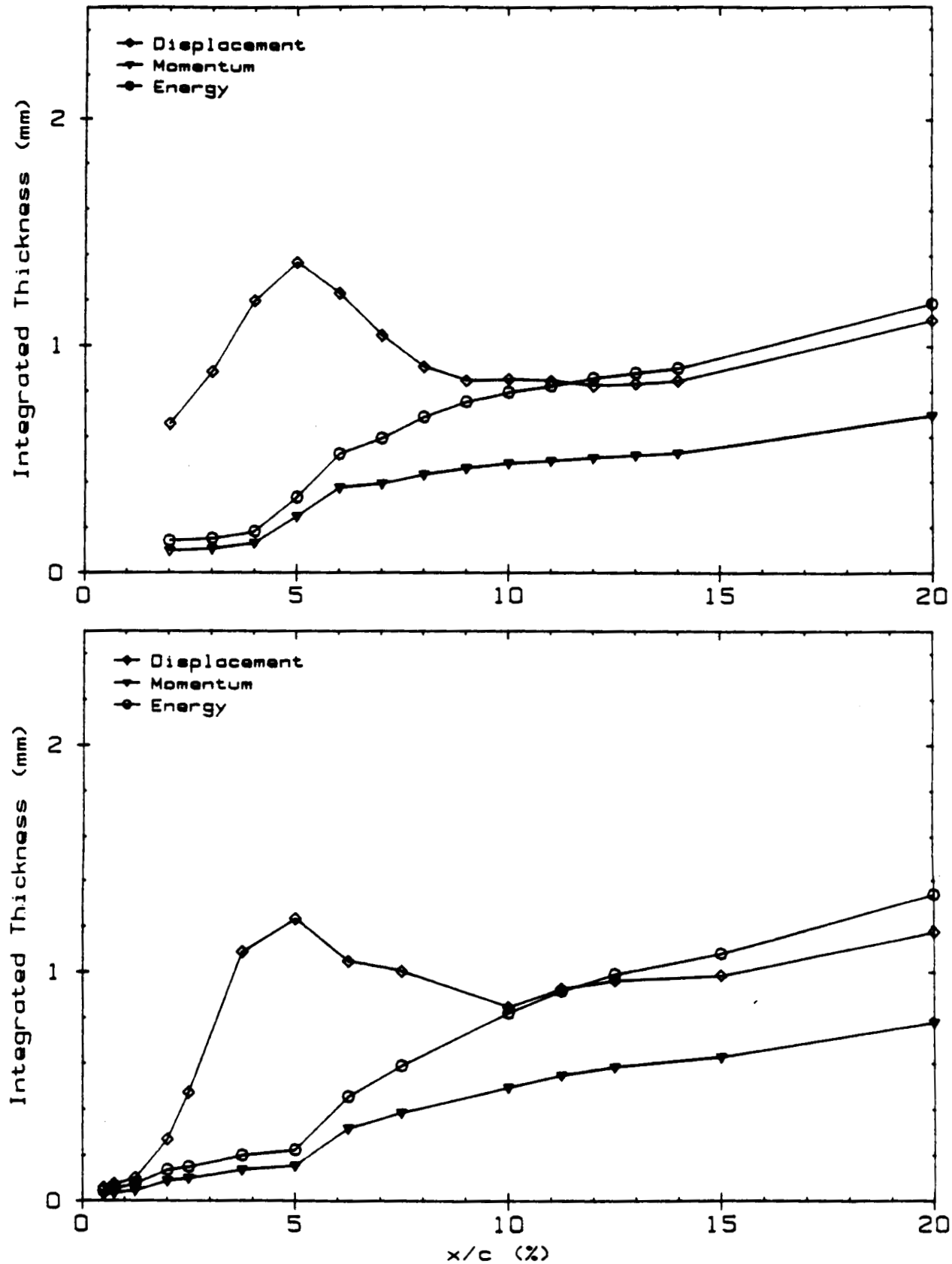

Figure 4. Integrated Boundary Layer Parameters on NACA 66_3-018 Airfoil, R_c= 200,000, α = 12°, 0 Flow Restrictors; Fitzgerald Data (top), O'Meara Data (bottom).

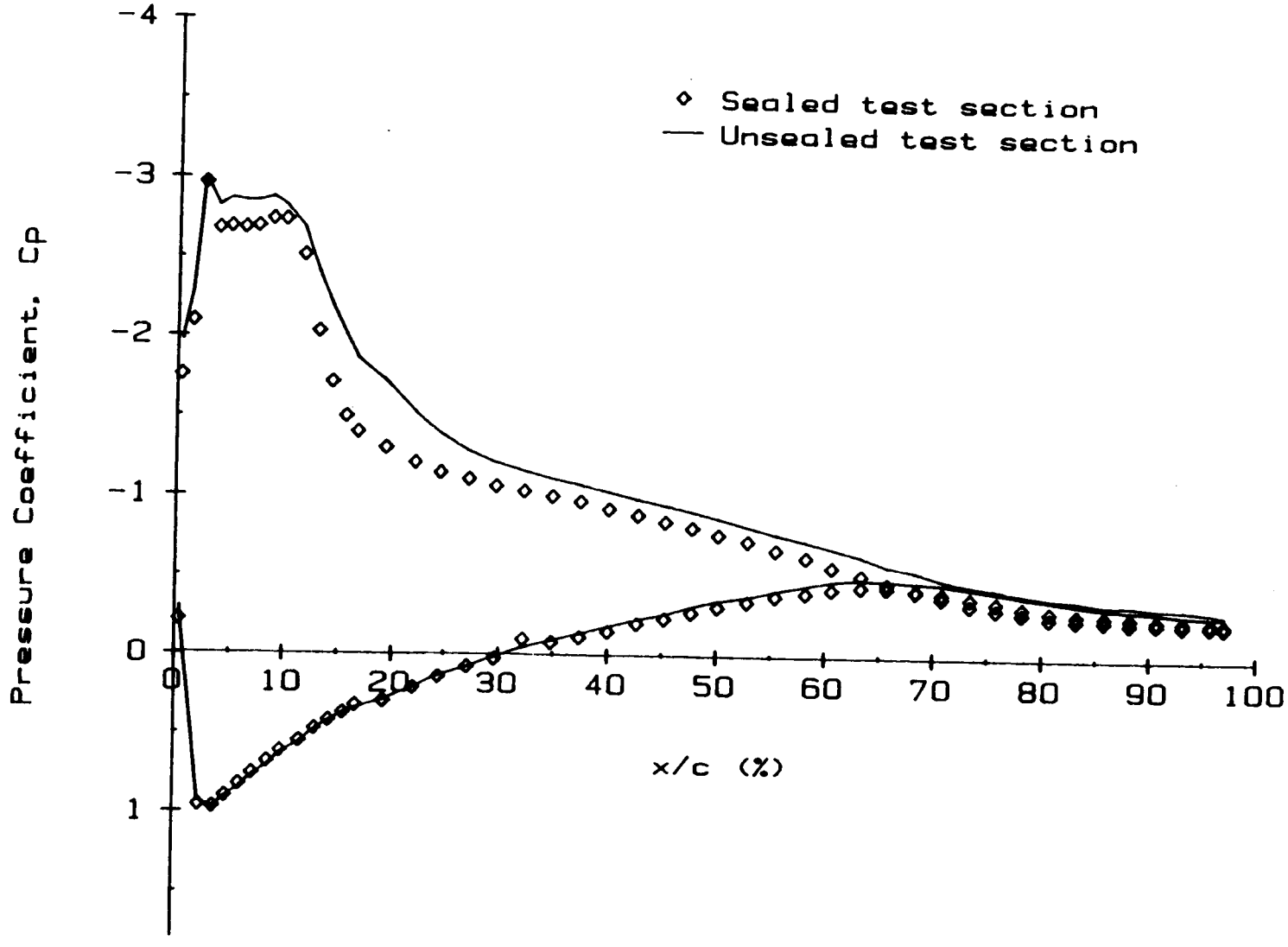

Figure 5. Pressure Distribution Comparison for Sealed and Unsealed Test Sections, R_c= 140,000, α = 12.°, 0 Flow Restrictors.

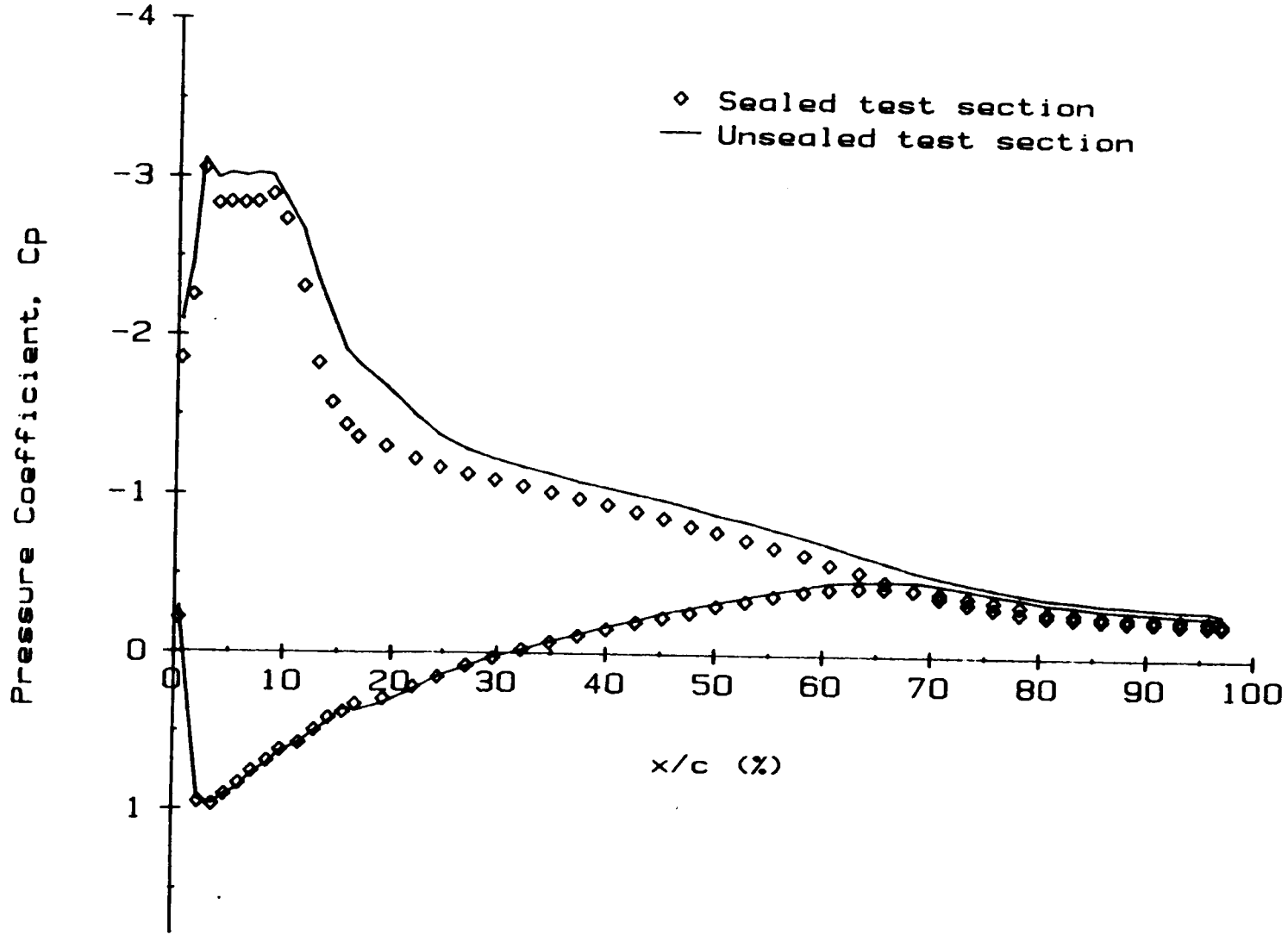

Figure 6. Pressure Distribution Comparison for Sealed and Unsealed Test Sections, R_c= 160,000, α = 12.°, 0 Flow Restrictors.

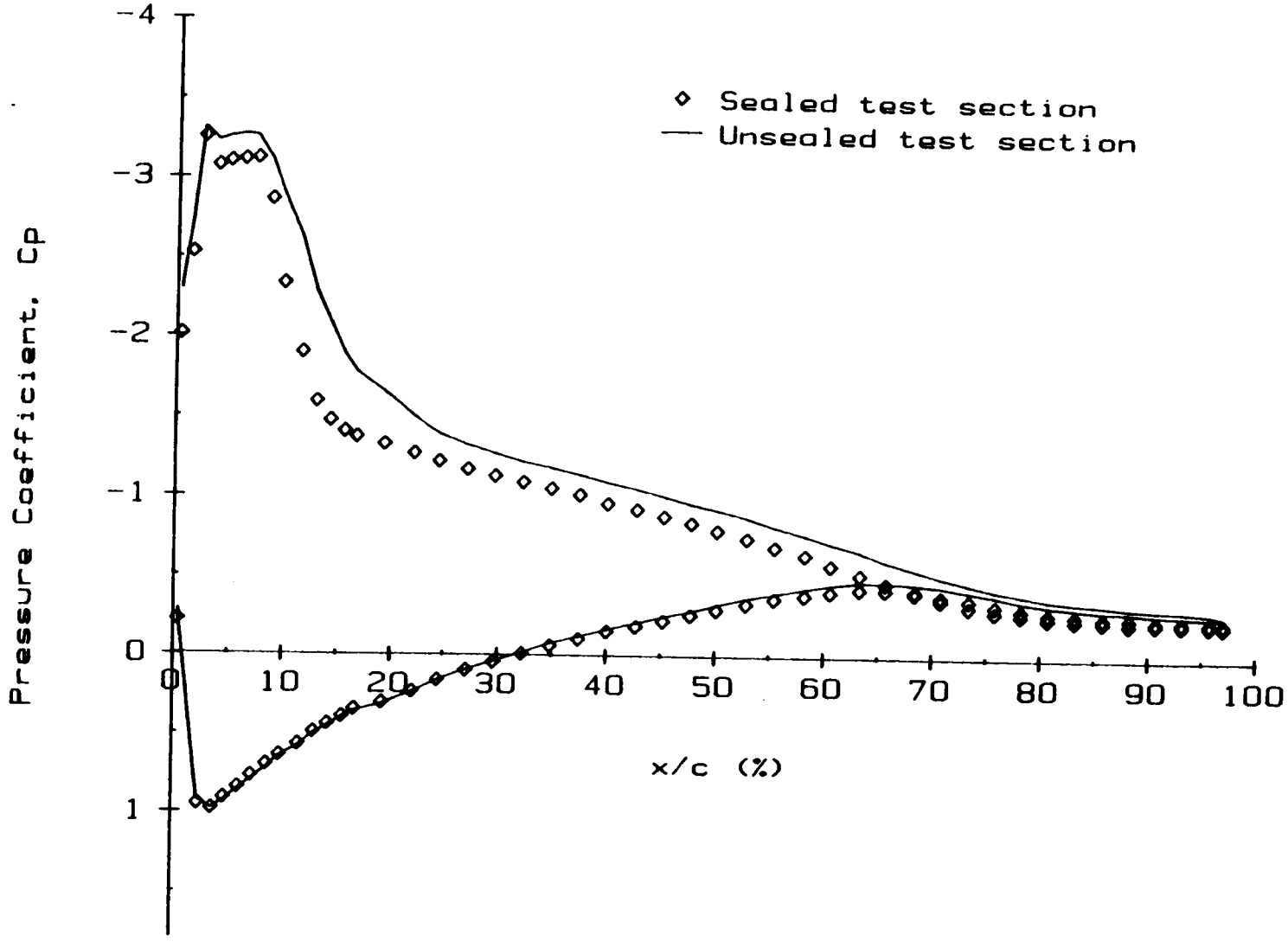

Figure 7. Pressure Distribution Comparison for Sealed and Unsealed Test Sections, R_c= 200,000, α = 12.°, 0 Flow Restrictors.

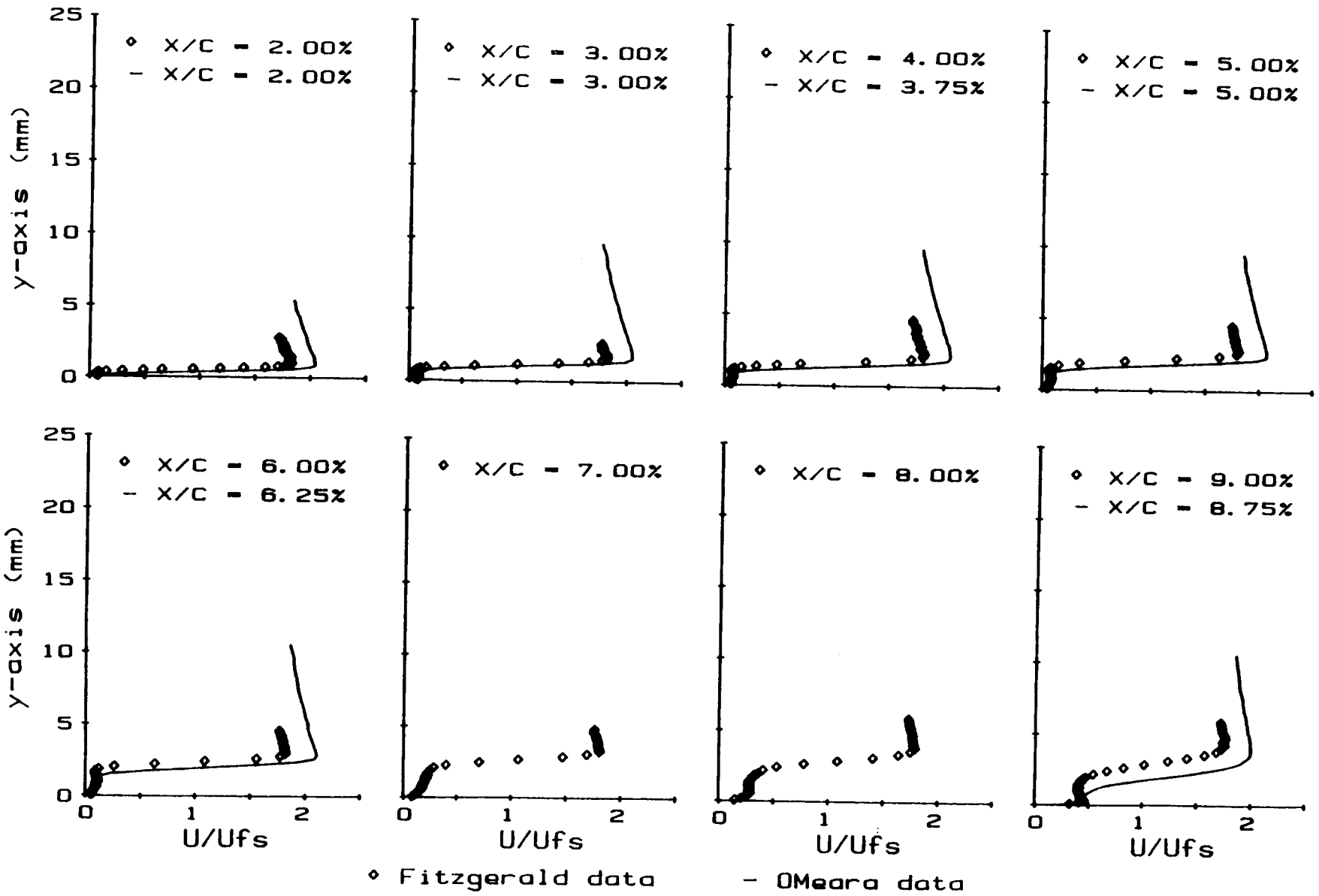

Figure 8a. Non-Dimensional Velocity Profiles (U/U_{fs}), x/c = 2.- 9.%, R_c = 140,000, α = 12°, 0 Flow Restrictors.

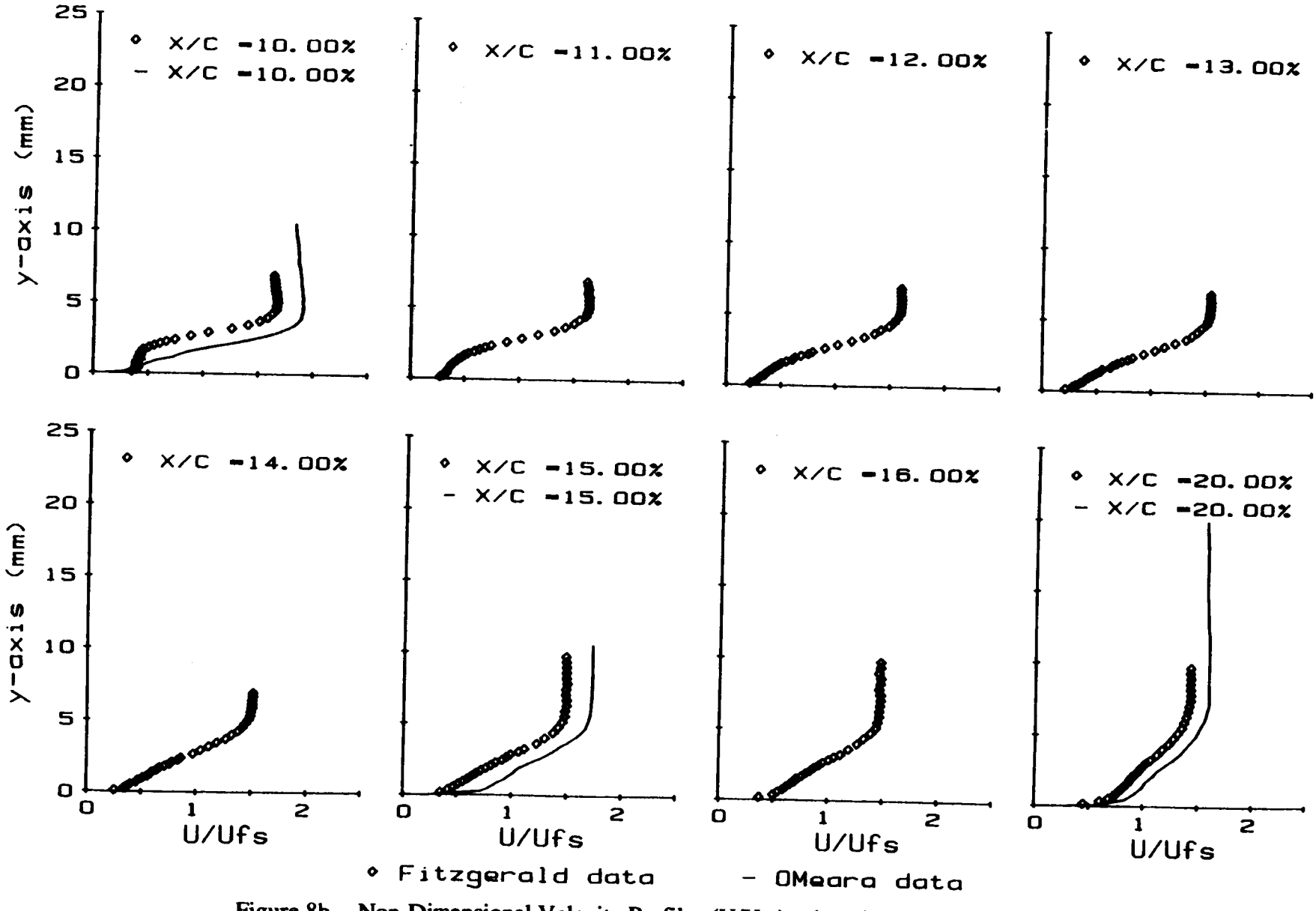

Figure 8b. Non-Dimensional Velocity Profiles (U/U_{fs}), x/c =10.- 20.%, R_c = 140,000, α = 12°, 0 Flow Restrictors.

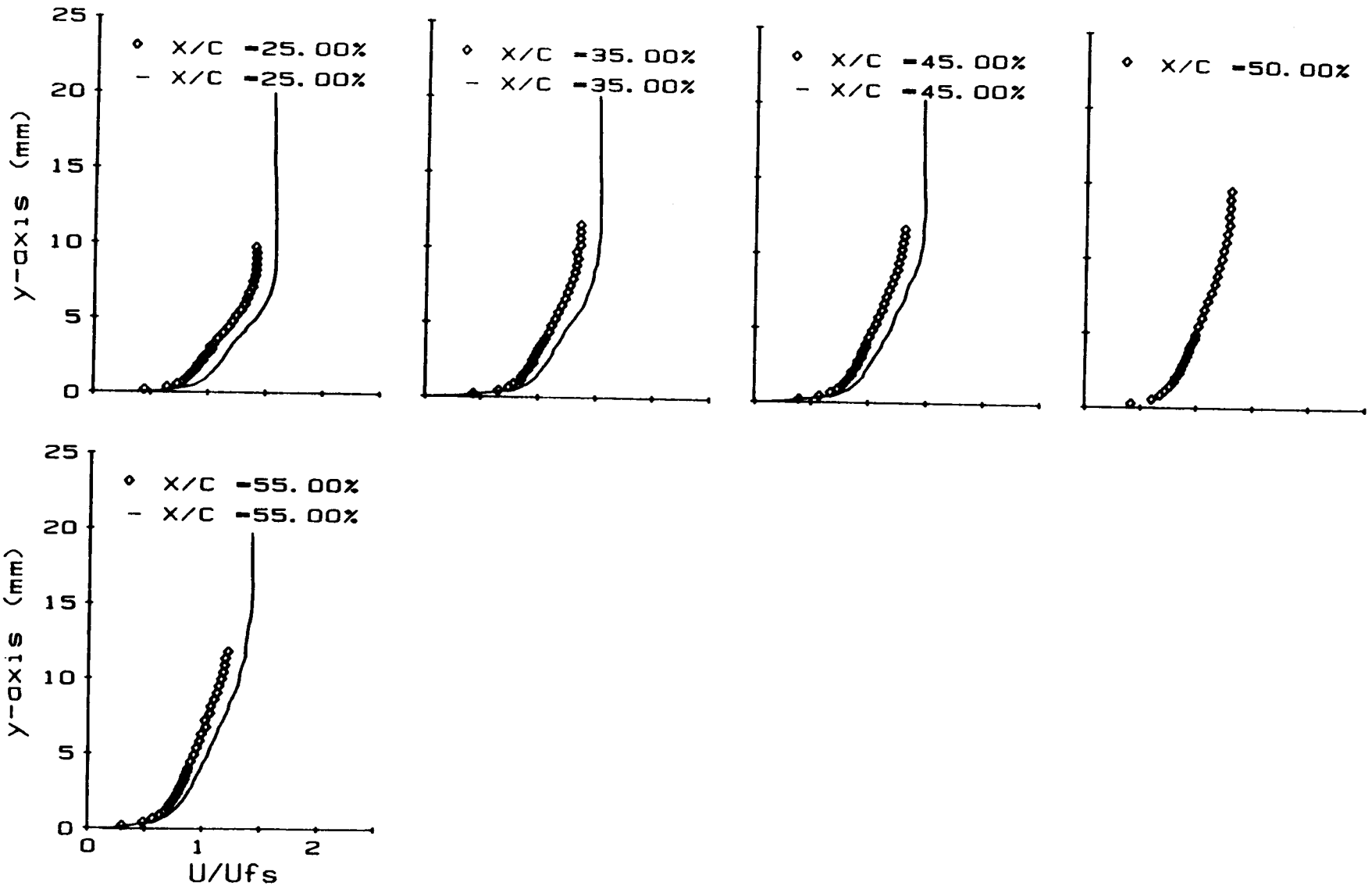

Figure 8c. Non-Dimensional Velocity Profiles (U/U_{fs}), x/c = 25.- 55.%, R_c = 140,000, α = 12°, 0 Flow Restrictors.

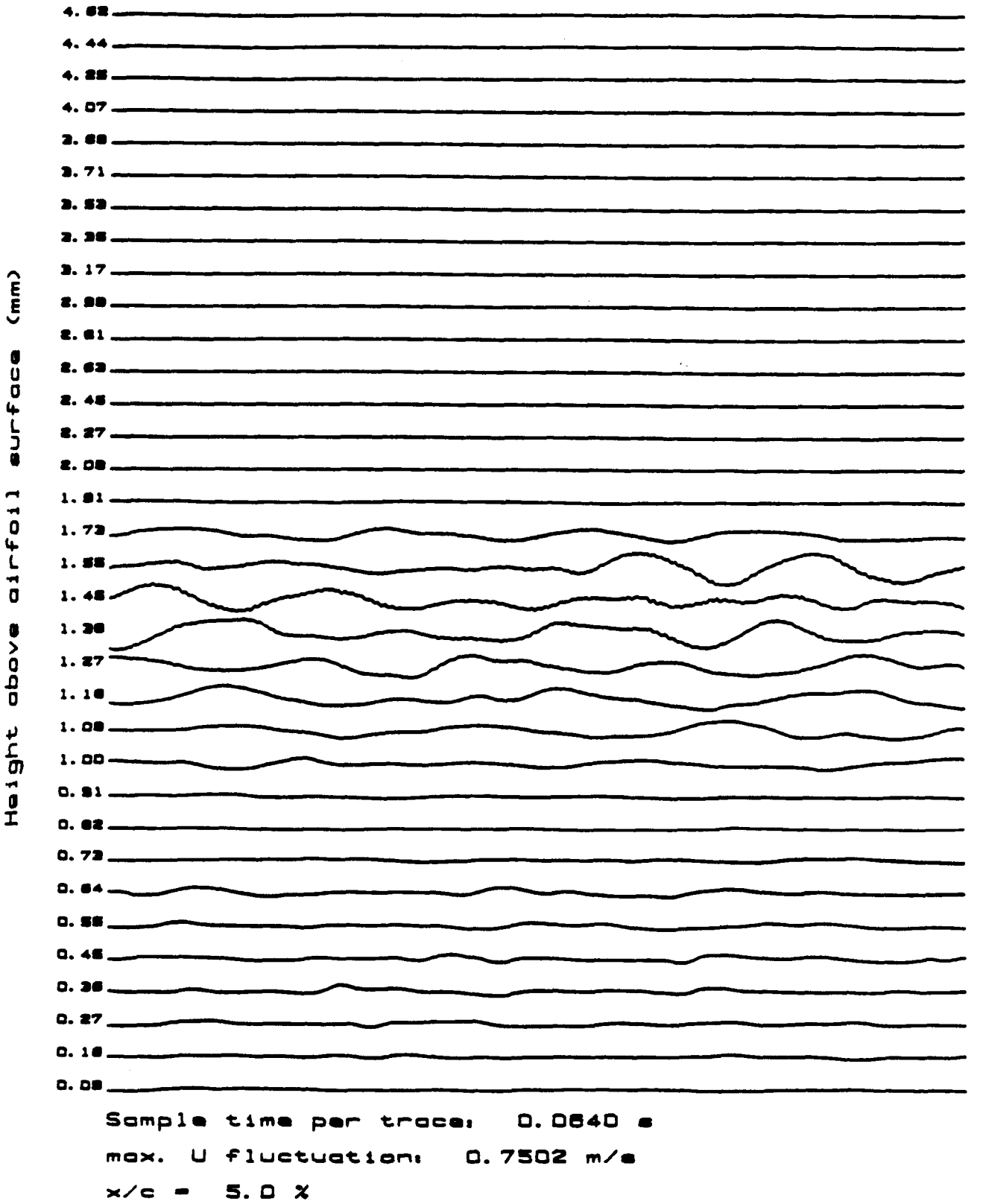

Figure 9a. Boundary Layer Velocity Fluctuations, x/c = 5.%, R_c=140,000, α = 10°, 0 Flow Restrictors, Acoustically Unforced.

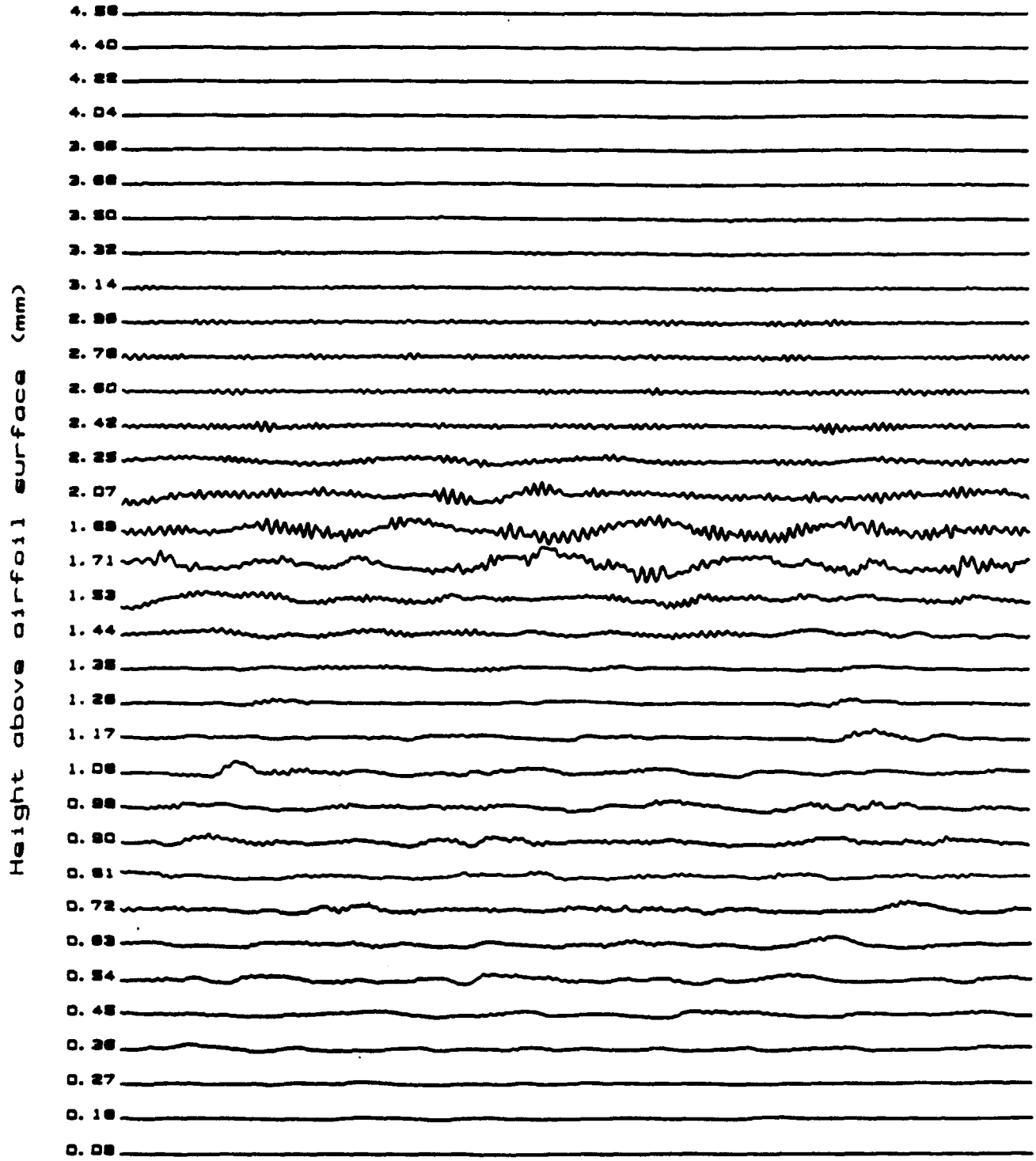

Figure 9b. Boundary Layer Velocity Fluctuations, x/c = 7.%, R_c=140,000, α = 10°, 0 Flow Restrictors, Acoustically Unforced.

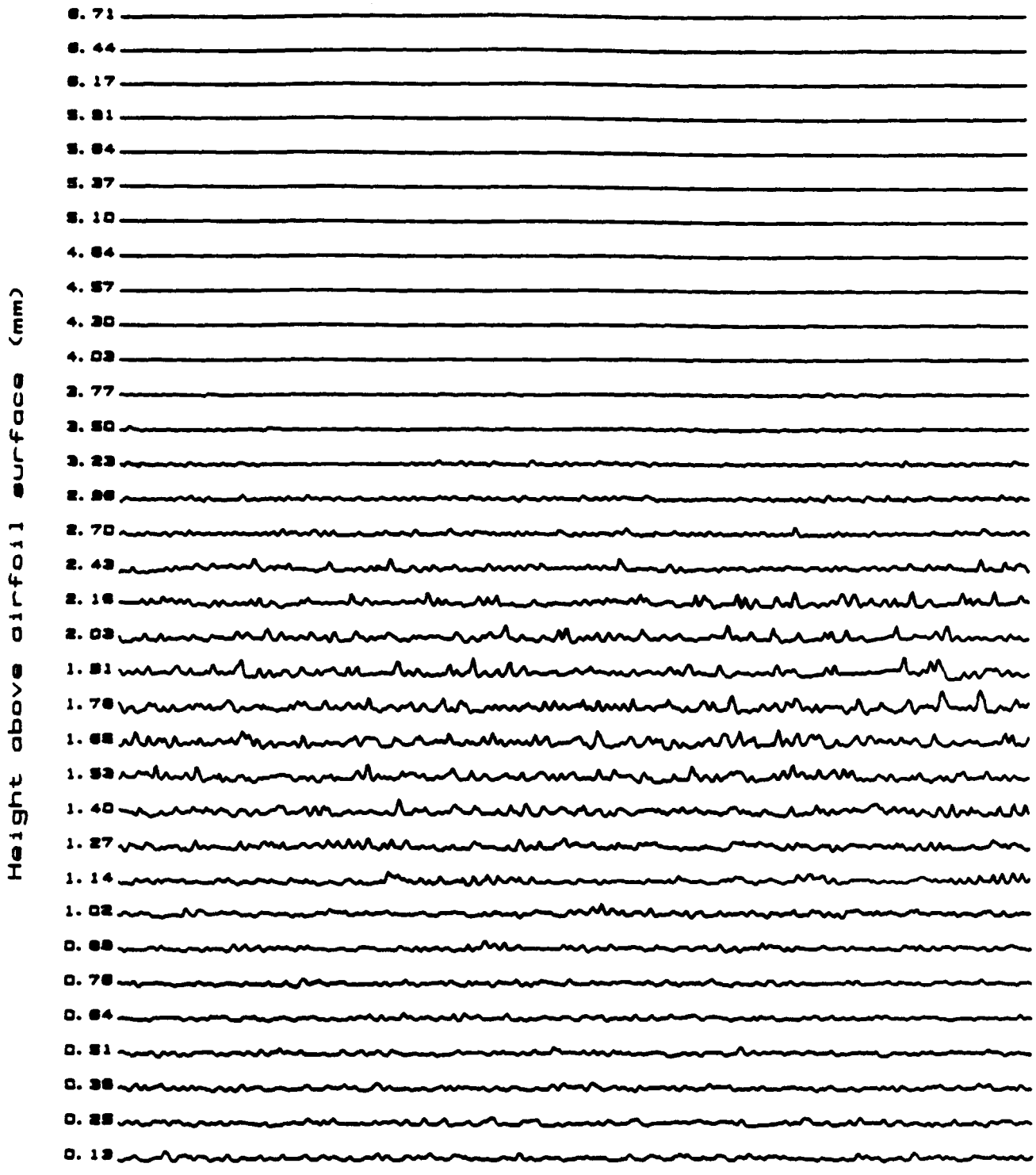

Figure 9c. Boundary Layer Velocity Fluctuations, x/c = 10.%, R_c=140,000, α = 10°, 0 Flow Restrictors, Acoustically Unforced.

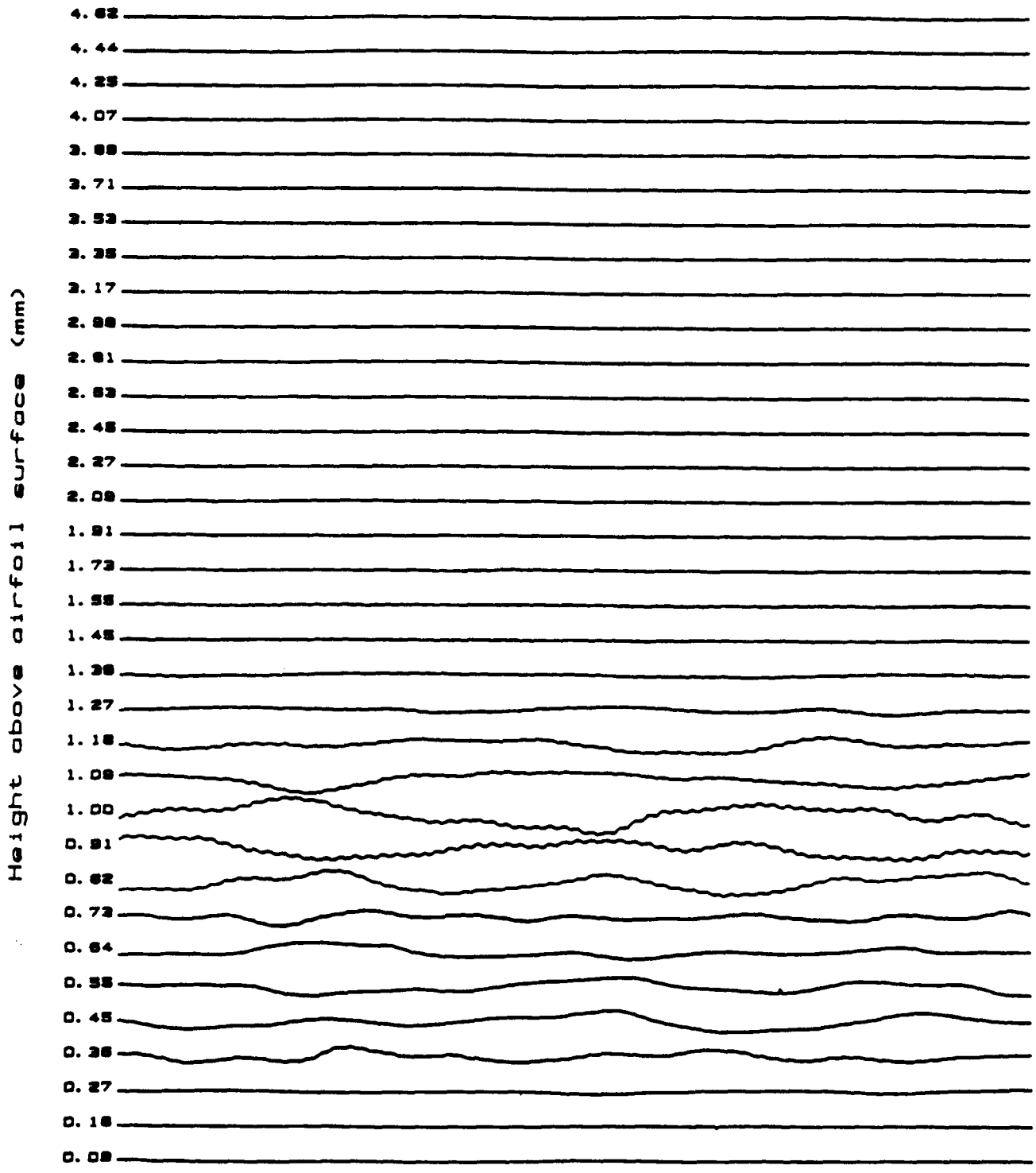

Figure 10a. Boundary Layer Velocity Fluctuations, x/c = 5.%, R_c= 140,000, α = 10°, 0 Flow Restrictors, Acoustic Forcing = 1623. Hz.

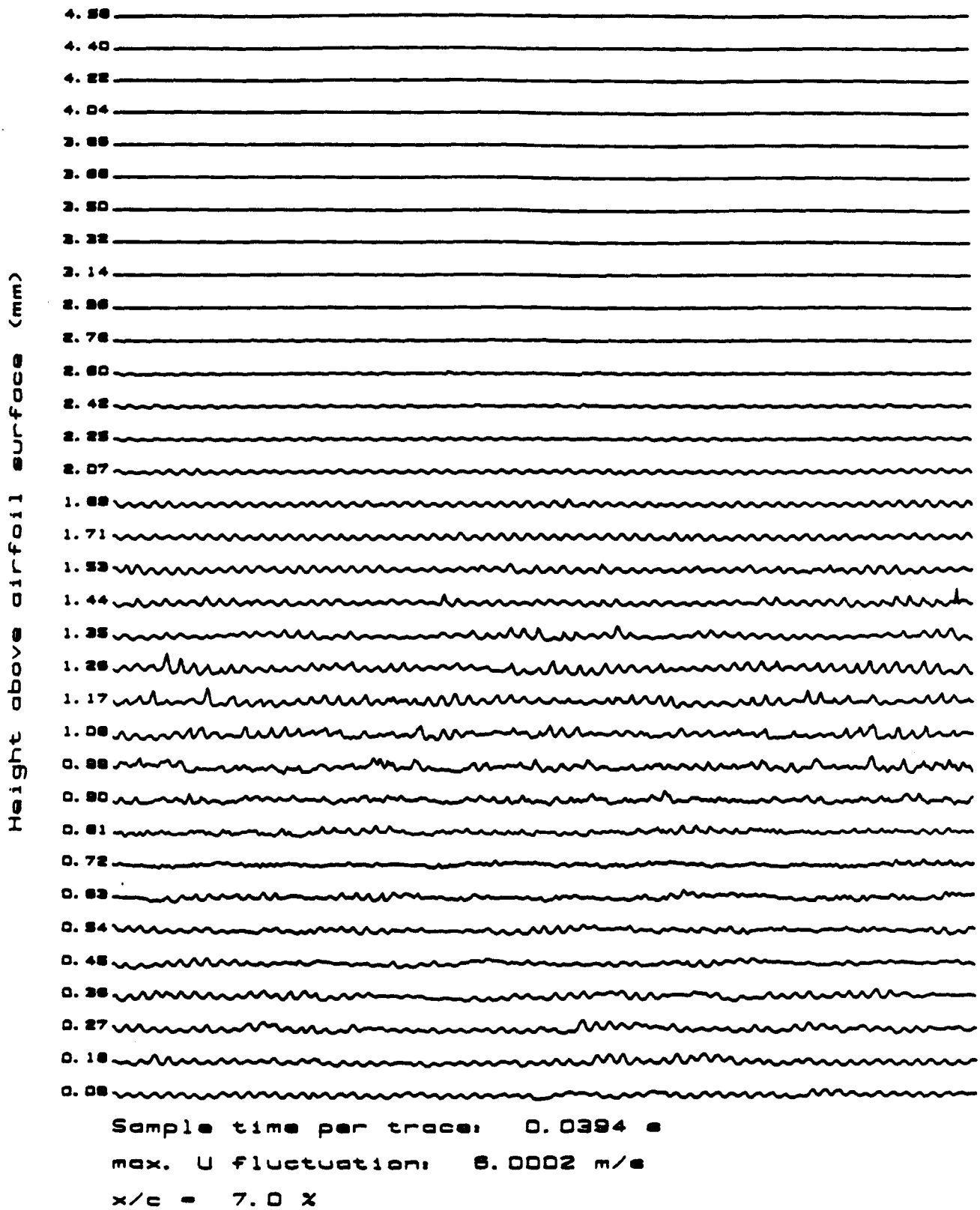

Figure 10b. Boundary Layer Velocity Fluctuations, x/c = 7.%, R_c= 140,000, α = 10°, 0 Flow Restrictors, Acoustic Forcing = 1623. Hz.

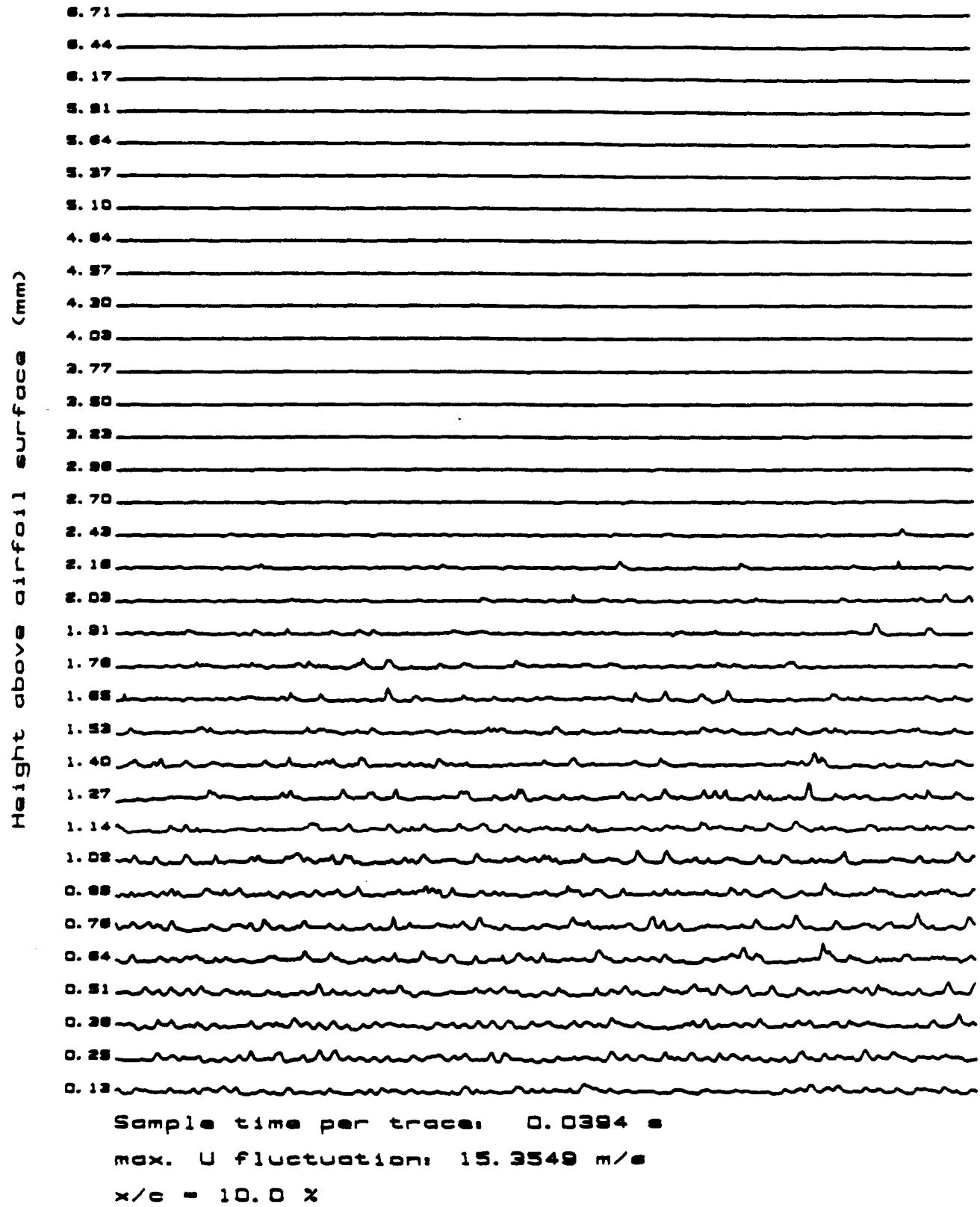

Figure 10c. Boundary Layer Velocity Fluctuations, x/c = 10.%, R_c= 140,000, α = 10°, 0 Flow Restrictors, Acoustic Forcing = 1623. Hz.

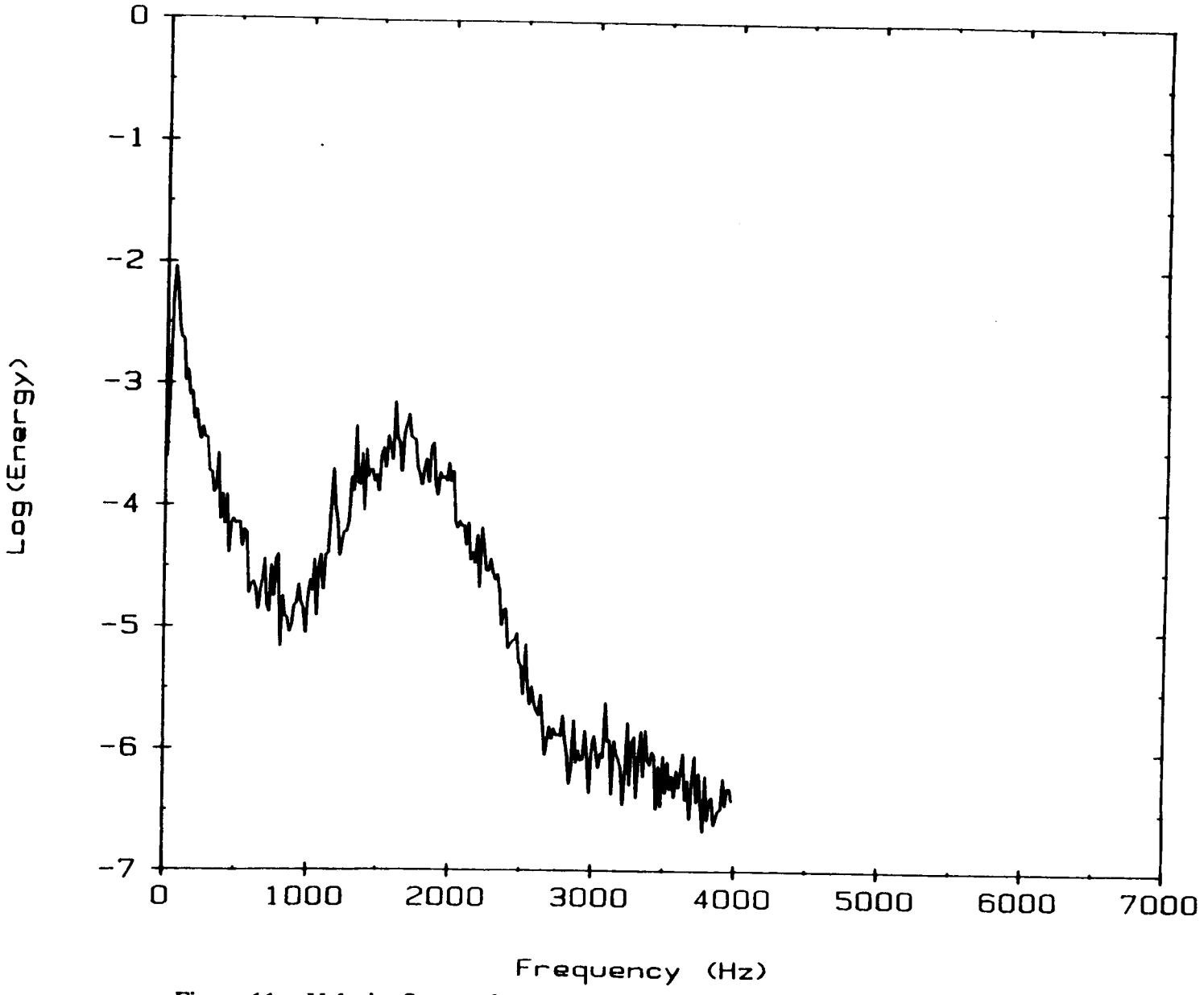

Figure 11. Velocity Spectra for Boundary Layer Profile, x/c = 7.%, R_c= 140,000, α =10°, 0 Flow Restrictors, Acoustically Unforced.

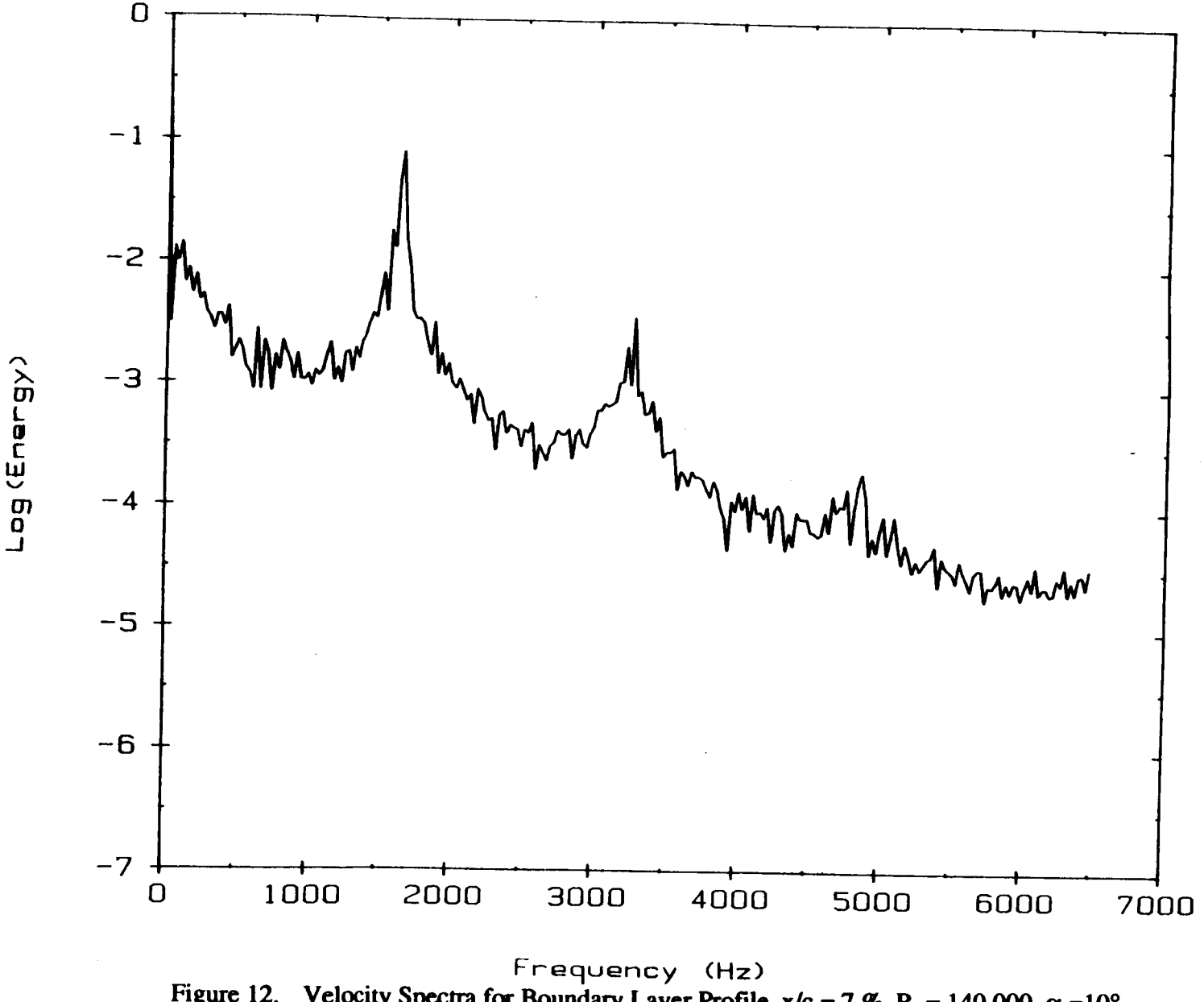

Figure 12. Velocity Spectra for Boundary Layer Profile, x/c = 7.%, R_c= 140,000, α =10°, 0 Flow Restrictors, Acoustic Forcing = 1623. Hz.

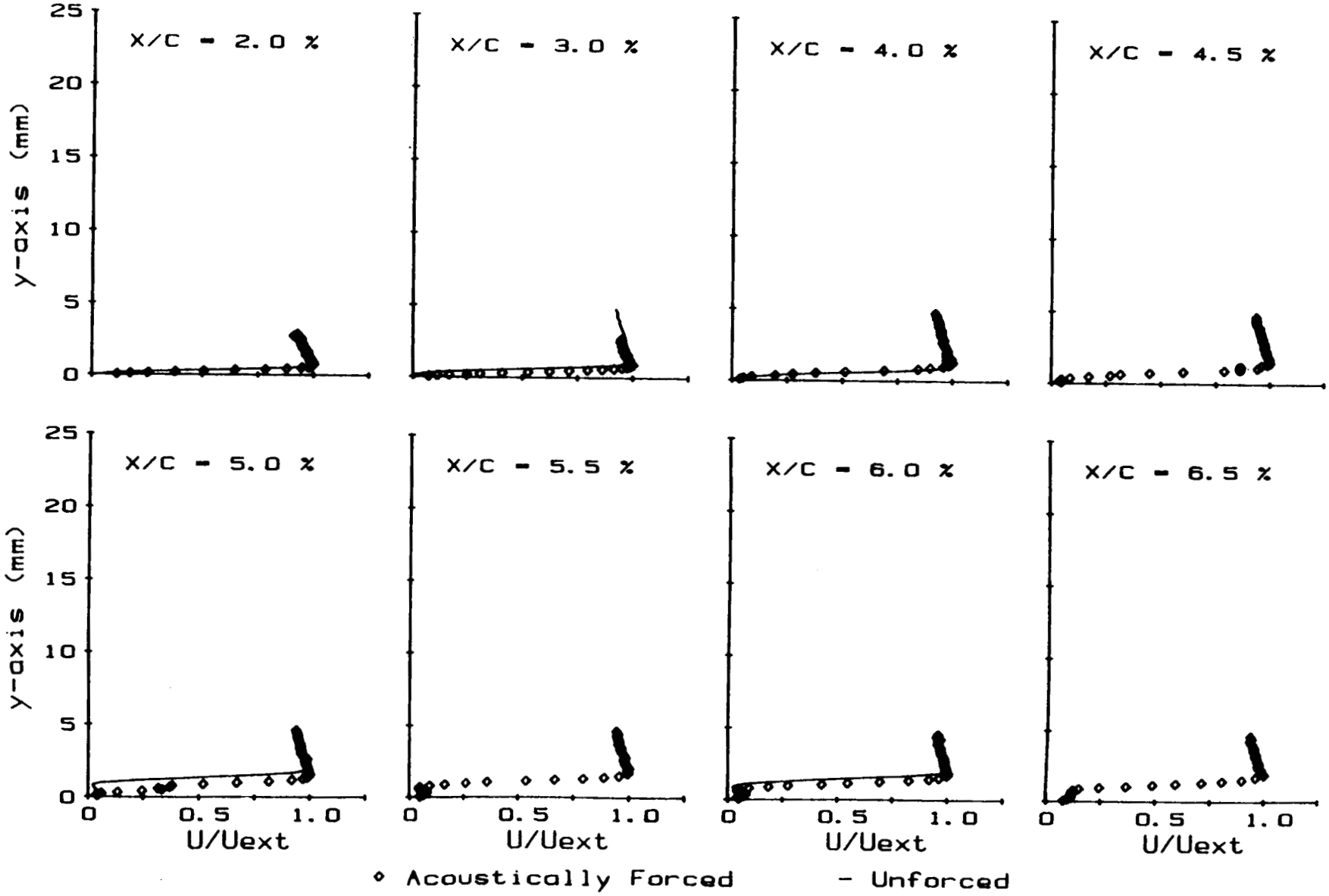

Figure 13a. Effect of Acoustic Forcing on Non-Dimensional Velocity Profiles (U/U_{ext}),
x/c = 2.0 - 6.5%, R_c = 140,000, α = 10°, 0 Flow Restrictors,
Acoustic Forcing = 1623 Hz.

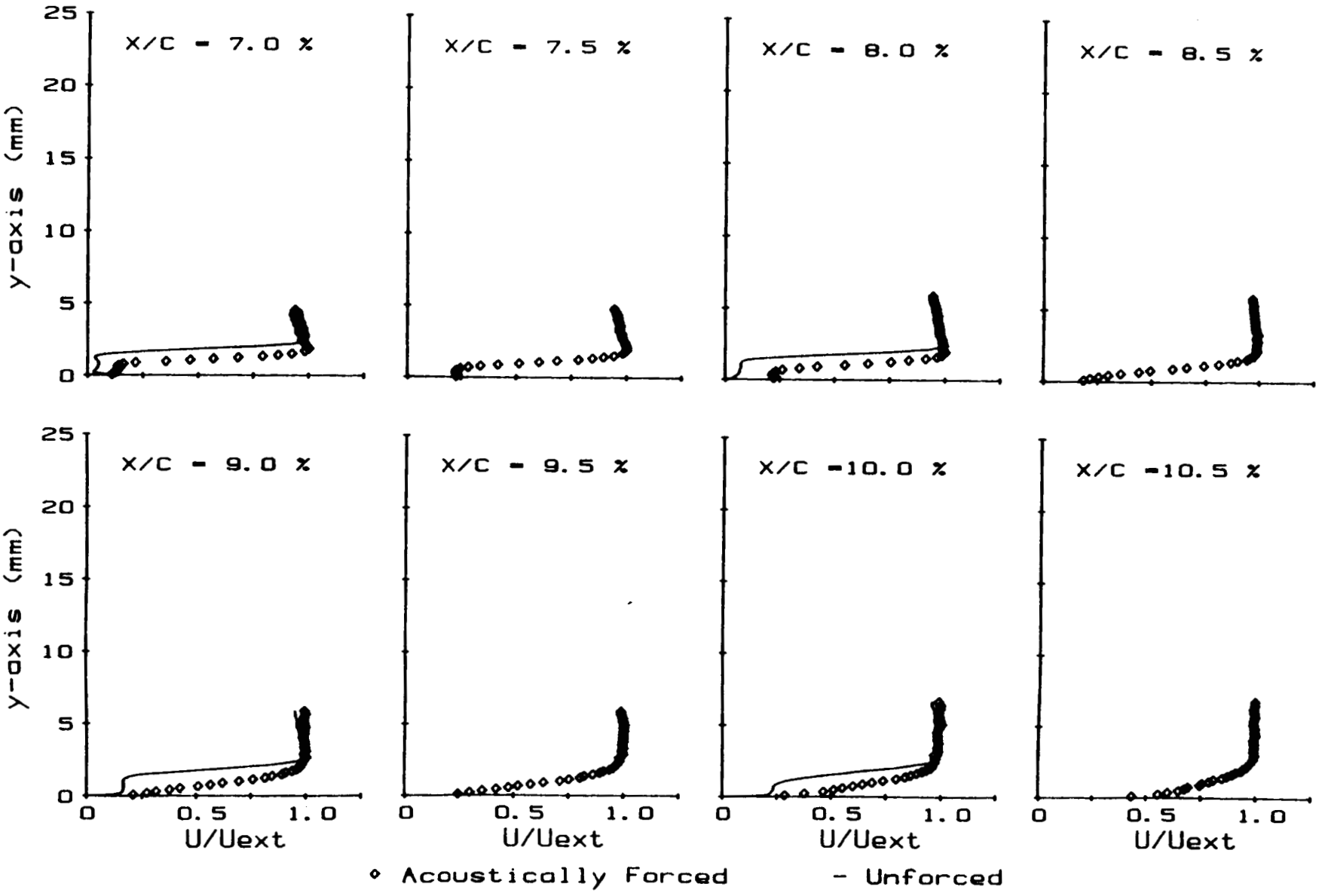

Figure 13b. Effect of Acoustic Forcing on Non-Dimensional Velocity Profiles (U/U_{ext}),
x/c = 7.0 - 10.5%, R_c = 140,000, α = 10°, 0 Flow Restrictors,
Acoustic Forcing = 1623 Hz.

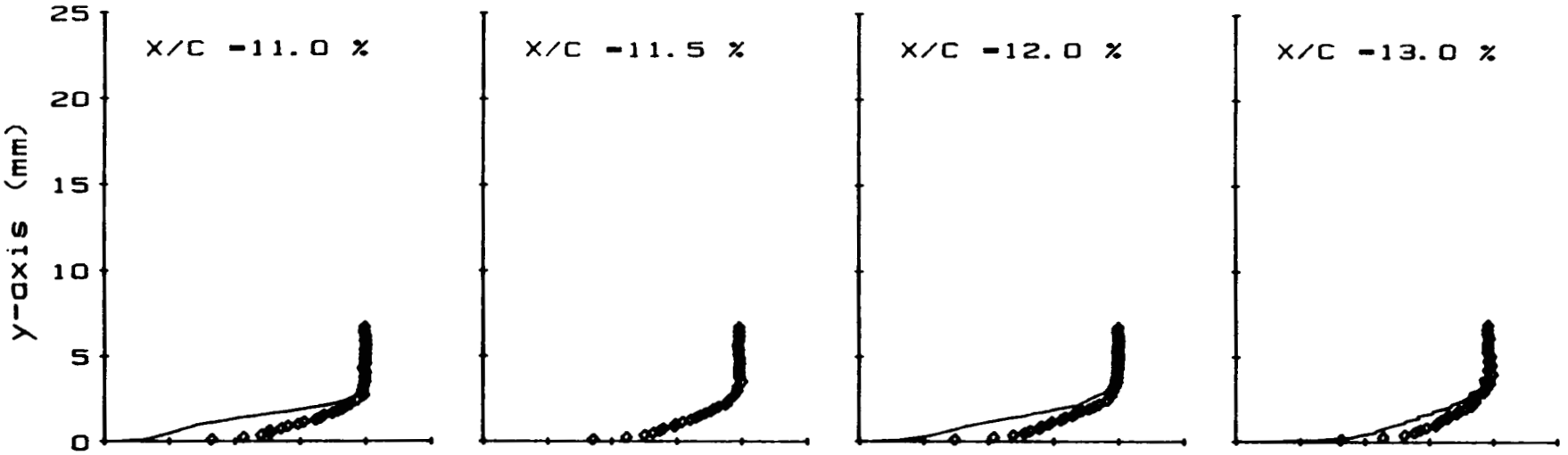

◇ Acoustically Forced — Unforced

Figure 13c. Effect of Acoustic Forcing on Non-Dimensional Velocity Profiles (U/U_{ext}), $x/c = 11.0 - 13.0\%$, $R_c = 140{,}000$, $\alpha = 10°$, 0 Flow Restrictors, Acoustic Forcing = 1623 Hz.

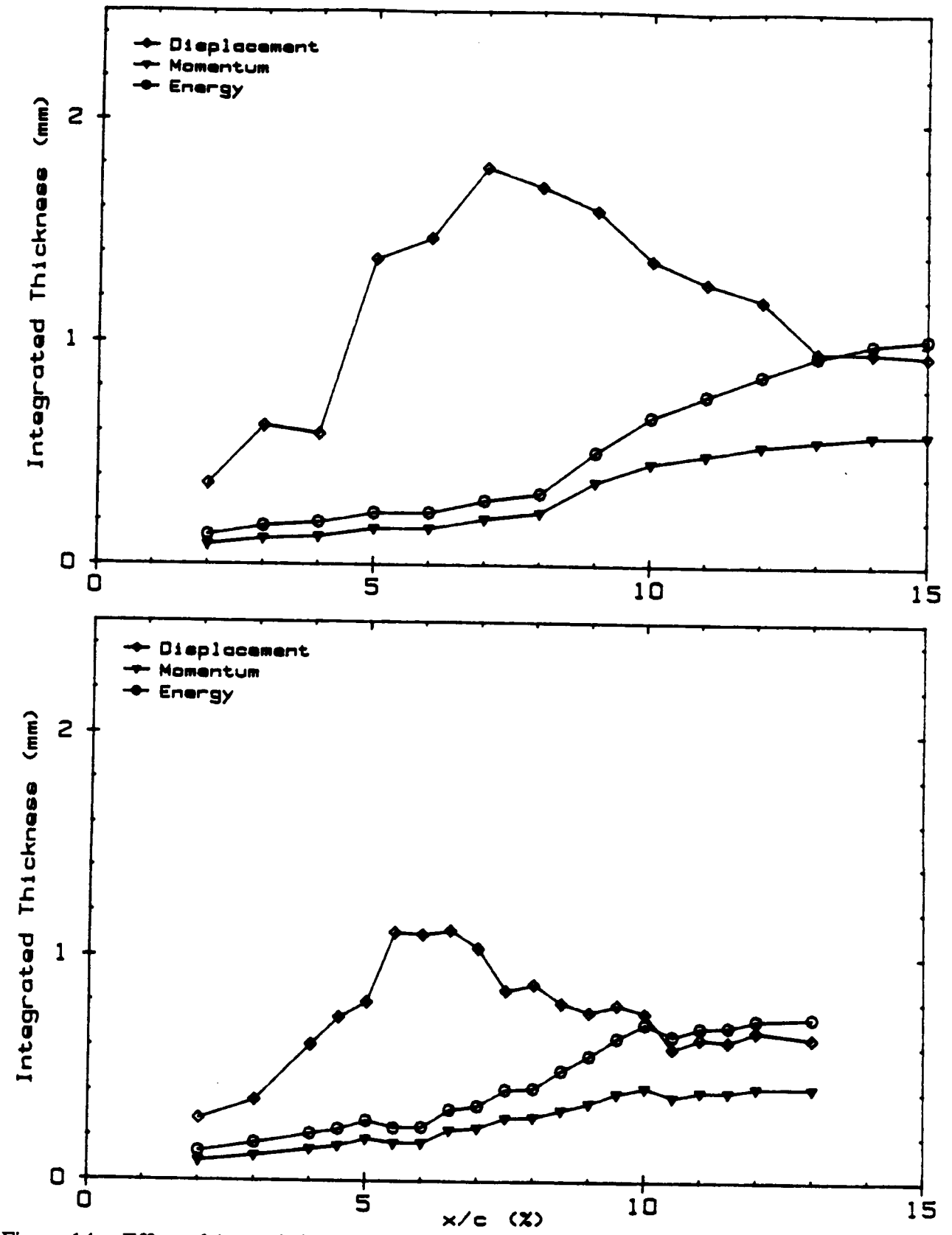

Figure 14. Effect of Acoustic Forcing on Integrated Boundary Layer Parameter Development, R_c= 140,000, α = 10°, 0 Flow Restrictors; Unforced (top), Acoustic Forcing = 1623 Hz. (bottom).

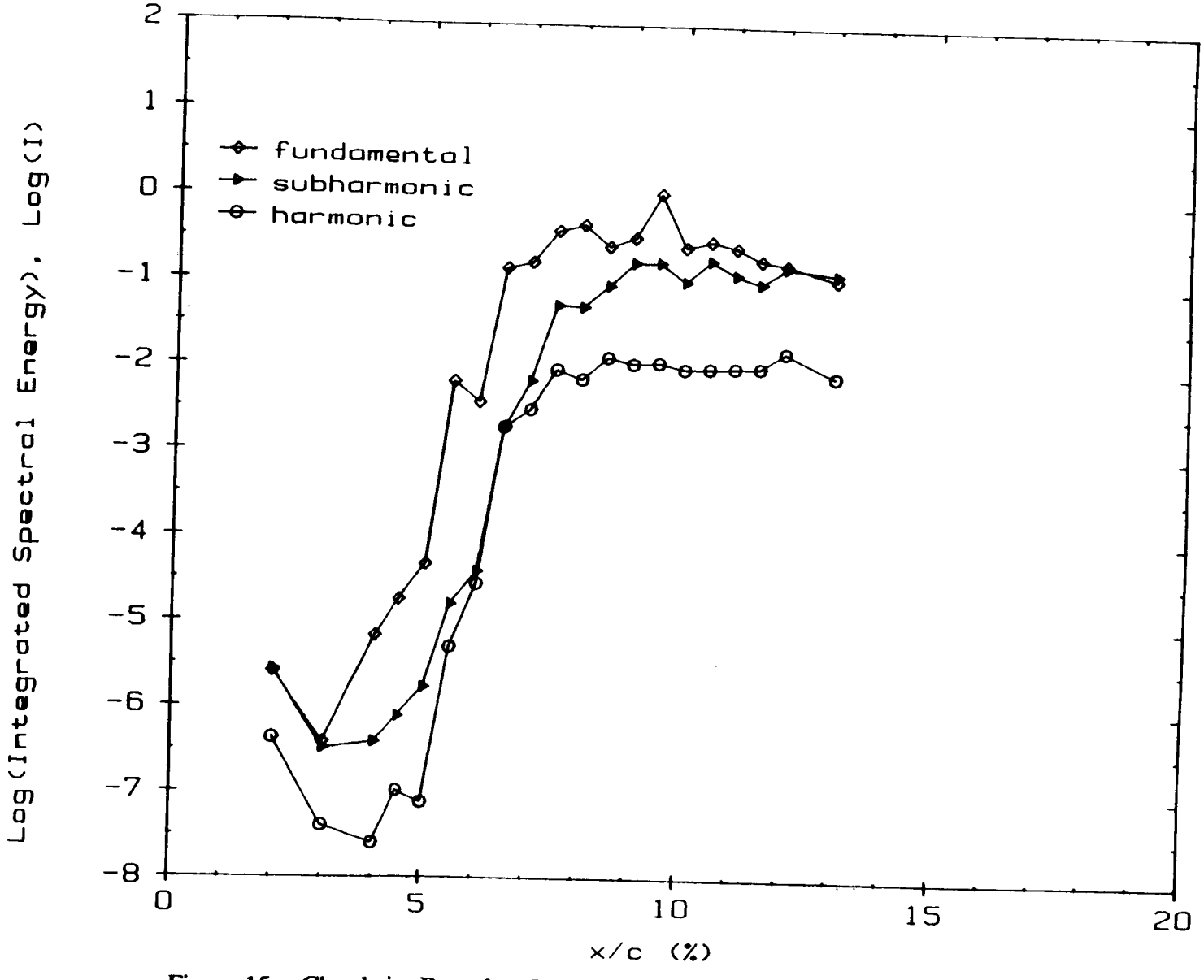

Figure 15. Chordwise Boundary Layer Modal Energy Development, R_c= 140,000, α = 10°, 0 Flow Restrictors, Acoustic Forcing = 1623 Hz.